



**HAL**  
open science

## Metalloprotease-mediated cleavage of CD95 Ligand

Vesna Risso, Mélissa Thomas, Blandine Guével, Regis Lavigne, Emmanuelle Com, Sophie Martin, Manon Nivet, Charles Pineau, Luc Negroni, Elodie Lafont, et al.

► **To cite this version:**

Vesna Risso, Mélissa Thomas, Blandine Guével, Regis Lavigne, Emmanuelle Com, et al.. Metalloprotease-mediated cleavage of CD95 Ligand. FEBS Journal, 2023, 290 (12), pp.3145-3164. 10.1111/febs.16737 . hal-03968369

**HAL Id: hal-03968369**

**<https://hal.science/hal-03968369v1>**

Submitted on 14 Feb 2025







**HAL** is a multi-disciplinary open access archive for the deposit and dissemination of scientific research documents, whether they are published or not. The documents may come from teaching and research institutions in France or abroad, or from public or private research centers.

L'archive ouverte pluridisciplinaire **HAL**, est destinée au dépôt et à la diffusion de documents scientifiques de niveau recherche, publiés ou non, émanant des établissements d'enseignement et de recherche français ou étrangers, des laboratoires publics ou privés.



Distributed under a Creative Commons Attribution - NonCommercial 4.0 International License

# Metalloprotease-mediated cleavage of CD95 ligand

Vesna Risso<sup>1,2</sup> , Mélissa Thomas<sup>3</sup>, Blandine Guével<sup>4,5</sup>, Regis Lavigne<sup>4,5</sup>, Emmanuelle Com<sup>4,5</sup>, Sophie Martin<sup>1,2</sup>, Manon Nivet<sup>1,2</sup> , Charles Pineau<sup>4,5</sup>, Luc Negroni<sup>6</sup>, Élodie Lafont<sup>1,2</sup> , Éric Chevet<sup>1,2</sup> , Leif A. Eriksson<sup>3</sup>  and Matthieu Le Gallo<sup>1,2</sup> 

1 Inserm UMR\_S 1242, Oncogenesis Stress Signalling, University of Rennes, France

2 Centre de lutte contre le Cancer Eugène Marquis, Rennes, France

3 Department of Chemistry and Molecular Biology, Lundberg Lab, University of Gothenburg, Sweden

4 Univ Rennes, Inserm, EHESP, Irset (Institut de recherche en santé, environnement et travail) – UMR\_S 1085, Rennes cedex, France

5 Protim, Univ Rennes, Rennes cedex, France

6 Inserm UMR\_S 1258, The Institute of Genetics and of Molecular and Cellular Biology (IGBMC), Université de Strasbourg, France

## Keywords

CD95 ligand; CD95L; metalloproteases; proteolytic cleavage; soluble CD95L

## Correspondence

M. Le Gallo, Inserm UMR\_S 1242, Oncogenesis Stress Signalling, University of Rennes, Rennes, France  
 E-mail: [matthieu.legallo@univ-rennes1.fr](mailto:matthieu.legallo@univ-rennes1.fr)

(Received 21 February 2022, revised 30 October 2022, accepted 23 January 2023)

doi:10.1111/febs.16737

CD95 is a member of the TNF receptor superfamily that is ubiquitously expressed in healthy and pathological tissues. Stimulation of CD95 by its physiological ligand CD95L induces its oligomerization leading in turn to the transduction of either apoptotic or nonapoptotic signals. CD95L can exist as both membrane-anchored and soluble forms (sCD95L), the latter resulting from the proteolytic cleavage of the former. Candidate proteases able to achieve CD95L cleavage were identified as matrix metalloproteases (MMP) due to their demonstrated ability to cleave other TNF superfamily ligands. The main goal of this study was to systematically identify the MMP family members capable of cleaving CD95L and subsequently determine the corresponding cleavage sites. By using different orthogonal biochemical approaches and combining them with molecular modelling, we confirmed data from the literature regarding CD95L cleavage by MMP-3 and MMP-7. Moreover, we found that MMP-2 and MMP-12 can cleave CD95L and characterized their resulting cleavage sites. This study provides a systematic approach to analyse the cleavage of CD95L, which until now had only been poorly described.

## Introduction

The death receptor CD95 and its cognate ligand CD95L were first described for their implication in extrinsic apoptotic signal transmission. This couple has also been involved in the development of various diseases. CD95 is a 319-amino acids (aa) type I transmembrane (TM) glycoprotein, which, similar to the other members of the Tumour Necrosis Factor (TNF) receptor superfamily (e.g. TNFR1), is ubiquitously

expressed in both healthy and pathological tissues. Its natural ligand CD95L, also called FasL or CD178, is a 281-aa type II TM protein mainly expressed at the surface of cytotoxic T lymphocytes. The stimulation of CD95 by its physiological ligand induces CD95 oligomerization and the recruitment, via its death domain, of several proteins involved in the transduction of apoptotic signals [1].

## Abbreviations

ACN, acetonitrile; ADAM, A Disintegrin And Metalloprotease; CID, collision-induced dissociation; FDR, false discovery rate; FRET, fluorescence resonance energy transfer; GST, Glutathione S-Transferase; HRP, Horseradish Peroxidase; KO, Knockout; LC, liquid chromatography; MMP, matrix metalloproteinase; MS, mass spectrometry; PASEF, parallel accumulation-serial fragmentation; PDB, protein data bank; QTOF, Quadrupole Time-Of-Flight; SLE, systemic lupus erythematosus; TBST, Tris-buffered saline with 0.1% Tween 20 Detergent; THD, TNF homology domain; TIMS, trapped ion mobility spectrometry; TM, transmembrane; TMB, 3,3',5,5'-tetramethylbenzidine; TNF, tumour necrosis factor; TOF, Time Of Flight; WT, wild-type.

Over the past 20 years, several studies reported non-apoptotic signalling by the CD95L-CD95 system [2,3]. In some cases, the ability of CD95 to drive such non-apoptotic signalling outcomes was attributed to its binding to a soluble form of CD95L (sCD95L) to be identified [4–11]. The extracellular domain of CD95L shows a stalk region (aa 103–136) located between the TM domain (aa 81–102) and the TNF homology domain (THD) (aa 137–281), which can be proteolytically cleaved through the action of metalloproteases. This cleavage gives rise to a 20–25 kDa sCD95L, which adopts a trimeric conformation, suggesting that the membrane-bound form is likely cleaved once the self-assembly between three monomeric THDs is complete [12]. A trimeric sCD95L, coupled to the pre-assembled CD95 trimer, is sufficient to trigger the nonapoptotic signalling cascade (e.g. NF- $\kappa$ B, ERK or PI3K/Akt pathways activation, see Risso *et al.* for review) [13], while its membrane-bound counterpart requires a greater oligomerization order (i.e. homohexamers) to induce apoptotic signals [14]. sCD95L is released into the bloodstream [15–19]. High levels of sCD95L have been quantified in the serum of patients suffering from various types of pathologies including cancer, autoimmune diseases and chronic inflammation, and has been correlated with disease progression, but so far no causal association has been established [9,11,20–25]. According to several studies, sCD95L could be added to the diagnostic criteria of various autoimmune diseases as a potential biomarker for disease severity and might be used in the follow-up of these pathologies [26–29].

Although CD95L has been studied for the past 30 years, little is still known about the molecular and physiological mechanisms involved in the release of sCD95L. By analogy with the cleavage of other members of the TNF ligand superfamily [30–39], metalloproteases might mediate the cleavage of CD95L. Matrix metalloproteases (MMPs) are endopeptidases belonging to a large family of 28 members in vertebrates, 24 genes of which are found in human [40]. These proteases are for instance involved in the shedding of cell surface receptors and membrane-anchored proteins, the release of soluble ligands and the activation or inactivation of chemokines/cytokines. Furthermore, MMPs play an important role in tissue remodelling associated with various physiological and pathological processes, such as cell proliferation, migration, differentiation, angiogenesis, apoptosis and host defence against bacterial or viral infections [41–46].

Individual studies carried out in the early 2000 s revealed that a gelatinase (MMP-9) [18], a Stromelysin

(MMP-3) [17], a Matrilysin (MMP-7) [15] and A Disintegrin And Metalloproteinase domain-containing protein 10 (ADAM-10) [16,19], could all be responsible for CD95L cleavage. However, no systematic analysis of CD95L cleavage sites and the corresponding MMP responsible has been reported so far. Owing to the increasing evidence that targeting some of CD95L cleavage products could be physiopathologically relevant, the aim of this study was to determine, through a combination of biochemical and MS-based approaches, the exact MMP responsible for CD95L cleavage and the corresponding sites.

## Results

### Study of CD95L proteolysis by MMPs responsible for TNF $\alpha$ shedding

An extensive literature search showed that four metalloproteases MMP-3 [17], MMP-7 [15], MMP-9 [18] and ADAM-10 [16,19] could be involved in CD95L cleavage. However, these studies did not systematically screen for metalloproteases cleaving CD95L. To comprehensively explore the metalloproteases involved in CD95L cleavage, we built on the work carried out on TNF $\alpha$ , the most characterized ligand of the TNF superfamily. Indeed, the proteases previously described to cleave CD95L (MMP-3, 7, 9, ADAM-10 and ADAM-17) are among those involved in the cleavage of TNF $\alpha$  [31,33–37,39,47–49]. Consequently, we systematically assessed the proteolytic activity of the 13 enzymes that belong to the large metalloprotease and the associated ADAM families known to cleave TNF $\alpha$  (i.e., MMP-1, MMP-2, MMP-3, MMP-7, MMP-8, MMP-9, MMP-12, MMP-13, MMP-14, MMP-15, MMP-17, ADAM-10, ADAM-17). First, we determined the specific activity for each protease towards CD95L. The extracellular domain of CD95L in fusion with the Ig-like domain (Leukaemia Inhibitory Factor receptor gp190) [50], IgCD95L, was overexpressed in HEK 293 T cells. The Ig-Like domain of the protein confers an aggregated conformation mimicking that assumed by the membrane-bound CD95L. IgCD95L was incubated *in vitro* with the 13 TNF $\alpha$ -processing metalloproteinases. The proteases were used at concentrations that were calculated based on the specific activity provided by the manufacturers (Fig. S1a). The resulting proteolytic products were subsequently analysed by western blot (Fig. 1A, S1b). First, we identified a strong proteolytic activity of MMP-2, MMP-3, MMP-7 and MMP-12. In addition, a weaker signal was detected for MMP-1, MMP-13 and ADAM-17 even when using elevated amounts of proteases.

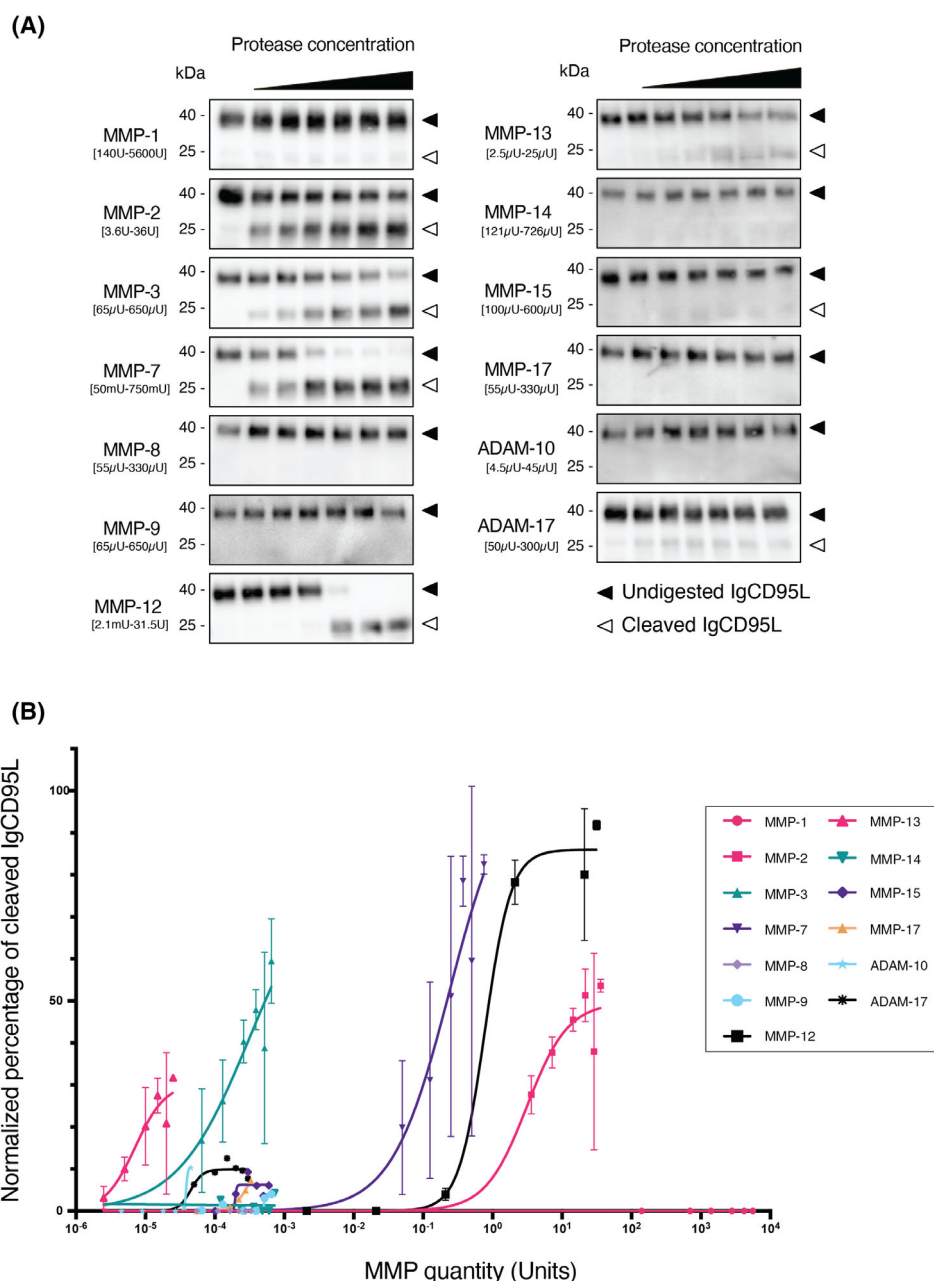


**Fig. 1.** Metalloprotease-mediated IgCD95L ectodomain cleavage. (A) Anti CD95L western blot of the proteolytic digestion of 150 pg of recombinant IgCD95L protein using increasing concentrations of metalloproteases. The concentration range indicated between brackets was determined according to each metalloprotease-specific activity and (Fig. S1b). Undigested IgCD95L was used as a negative control (left lane). Undigested full-length protein (40 kDa – black arrow) and C terminus-cleaved fragment of IgCD95L (around 23 kDa – light arrow) are indicated. One experiment representative of three is depicted. (B) Dot plot of the normalized quantity of IgCD95L cleaved calculated from the immunoblot band densitometry, according to the quantity of metalloproteases (in Units). Results are expressed as mean SD of three independent experiments. A nonlinear regression dose response model was fitted and a EC50 was calculated for each metalloprotease (Table S1a).

Densitometry analysis of the blots allowed us to determine an IgCD95L-specific EC50 for 10 out of the 13 metalloproteases (Fig. 1B, Table S1a). These results

were confirmed by performing *in vitro* cleavage on another CD95L substrate in fusion with Glutathione S-Transferase (GST) as described in Material and

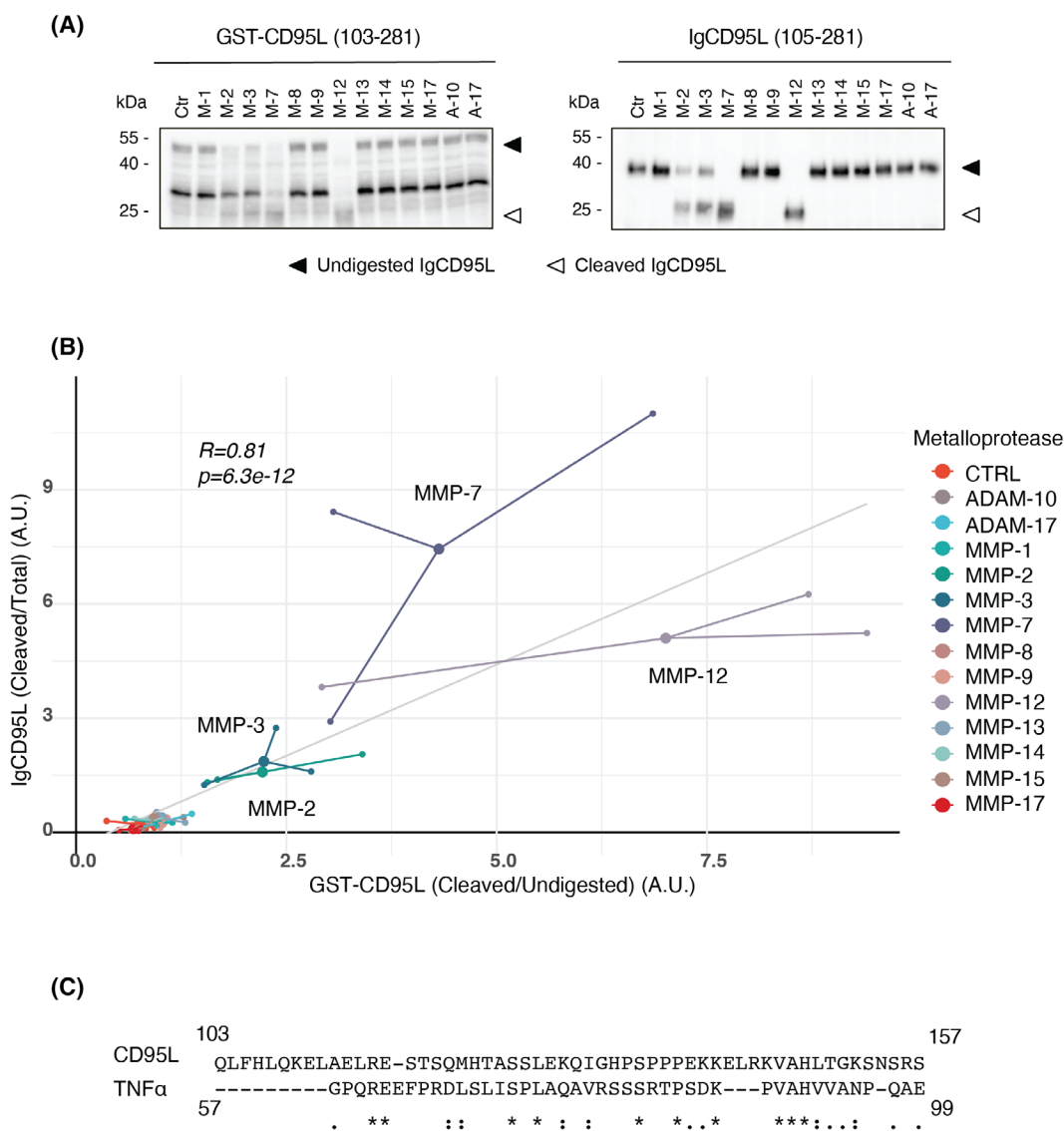


**Fig. 2.** Metalloprotease-mediated GST-CD95L ectodomain cleavage. (A) Anti CD95L western blot of the proteolytic digestion of recombinant GST-CD95L (right) and 150 pg of IgCD95L (left) proteins using an optimized quantity of metalloproteases determined in Fig. 1B, undigested recombinant proteins were used as negative control (left lane). Undigested full-length proteins (55 kDa: GST-CD95L, 40 kDa: IgCD95L – black arrow) and C terminus-cleaved fragments (around 23 kDa – light arrow) are indicated. One experiment representative of three is depicted. (B) Star plot representing the proteolysis of the two recombinant (Ig/GST) CD95L substrates. Relative proteolysis of the two substrates was determined by optical densitometry of western blot analyses performed in triplicate (small dots) and the median was calculated (large dots). To compare the proteolytic activity of the metalloproteases on the two substrates a regression line was fitted and a correlation coefficient calculated. (C) Amino acid sequence alignment of CD95L (identifier P48023/103–157) and TNF (identifier P01375/57–99) ectodomains. Bottom row indicated the sequence similarity score using Gonnet PAM 250 matrix. “\*” indicates fully conserved residues, “:” indicates conservation between groups of strongly similar properties (scoring > 0.5). “.” indicates conservation between groups of weakly similar properties (scoring  $\leq$  0.5).

Methods, using the CD95L-specific activity determined on the IgCD95L substrate (Table S1b). Western blot analysis showed both GST-CD95L and IgCD95L were effectively processed by MMP-3, MMP-7 as previously reported [15,17]. Furthermore, two additional endopeptidases MMP-2 and MMP-12 also exhibited a

proteolytic activity towards both Ig and GST-CD95L as confirmed by the good correlation observed on the two CD95L substrates (Fig. 2A,B). Even though CD95L shares approximately 25–30% sequence identity with TNF $\alpha$ , the ectodomains of CD95L and TNF $\alpha$  are poorly conserved. This is illustrated by the

low consensus between the cleavage regions, which can explain the different role played by the selected TNF $\alpha$  proteases in the two proteolytic processes (Fig. 2C).

The following step aimed at characterizing the cleavage sites on CD95L. First, we designed a series of three peptides (A, B, C) spanning the cleavage sites that were reported in previous studies [12,15,51]. Peptides A, B and C covered distinct sections of the amino acid sequence of the CD95L ectodomain, corresponding to the juxtamembrane stalk region and the first amino acids of the trimerization domain (THD) (Fig. 3A). A model of the trimeric protein was developed using the partial crystal structure of CD95L and the predicted structure from AlphaFold V2.0 to visualize the precise location and predicted conformation of these peptides (Fig. 3A). To test the proteolytic activity of the selected proteases, we used an *in vitro* assay monitoring the cleavage of molecular beacons built by flanking each peptide substrate with a fluorophore (Mca) on the N terminus and with a quencher (Dnp) on the C terminus (Fig. 3B, Table S1c). MMP-mediated cleavage of the peptides leads to the removal of the quencher, allowing the fluorophore to emit light. MMP-3, MMP-7, MMP-9 and ADAM-10, previously described to cleave CD95L, were used in the presence or absence of the broad-spectrum metalloprotease inhibitor GM6001 and the resulting fluorescence was measured (Fig. 3C). Fluorescence was detected after incubating peptide A with MMP-3 and MMP-7 but not with MMP-9 and ADAM-10. No cleavage-dependent fluorescence was detected for peptides B and C. Taken together these observations pointed towards the cleavage of CD95L by MMP-3 and MMP-7 but not by MMP-9 and ADAM-10, whereas the cleavage mediated by MMP-3 and MMP-7 occurred between position 107 and 117 of the protein in accordance with previous knowledge [15].

### Mapping of CD95L cleavage sites

Potential CD95L cleavage sites were previously reported in the literature [12,15,51]. The studies, however, contained incomplete information primarily based on immunoblotting, sequential deletions and mutagenesis approaches on selected proteases, and remain to be confirmed. In addition, western blot profiles of CD95L cleavage products showed bands of various sizes (Fig. 2A). To systematically identify potential CD95L cleavage sites within the region of interest, we used a suite of proteolytic cleavage site prediction softwares (i.e. SITEPREDICT, PROSPER, PROTEASIX and DEEPCLEAVE) [52–55]. The amino acid sequence of the CD95L ectodomain (amino acids 103–281) was analysed. We

hypothesized that cleavages occurring within the THD would prevent CD95L trimerization. Consequently, only the predicted cleavage sites in the Stalk region and the beginning of the THD (amino acids 103–157), with a specificity greater than 95%, were considered for the present study. A confidence index was adopted to select the physiologically most likely cleavage sites. All the cleavage sites previously described in the literature ( $_{110}\text{EL}_{111}$ ,  $_{113}\text{EL}_{114}$ ,  $_{126}\text{SL}_{127}$ ,  $_{129}\text{KQ}_{130}$ ,  $_{142}\text{EL}_{143}$ ) were identified by at least one of the *in silico* tools, and additional sites were also predicted (putative cleavage sites between each of the following amino acid pairs:  $_{103}\text{QL}_{104}$ ,  $_{106}\text{HL}_{107}$ ,  $_{120}\text{QM}_{121}$ ,  $_{130}\text{QI}_{131}$ ,  $_{138}\text{PE}_{139}$ ,  $_{139}\text{EK}_{140}$ ,  $_{145}\text{KV}_{146}$ ,  $_{148}\text{HL}_{149}$ ) (Fig. 4A).

To identify the MMPs involved in the processing of the predicted cleavage sites, two additional peptide substrates were designed encompassing the cleavage region and the beginning of the THD (i.e. Peptides D and E) (Fig. 4B). A trimeric membrane-anchored CD95L model was used to visualize the location and structure of these peptides. The five peptides (i.e. Peptides A, B, C, D and E) were designed to be used in a fluorescence-based assay as described above and were processed *in vitro* to validate the MMPs identified in Figs 1–3 as able to cleave CD95L (i.e. MMP-2, MMP-3, MMP-7, MMP-12). A strong proteolytic activity revealed by an elevated fluorescence intensity was detected with peptides A and E for all MMPs tested here. Furthermore, a milder proteolytic signal was detected when peptide B was incubated with MMP-2 and MMP-12, and a moderate signal was detected when peptide D was processed by MMP-7. No proteolytic activity was detected towards peptide C (Fig. 4C). This assay allowed us to restrict the localization of the cleavage sites of CD95L and confirm the metalloproteases involved in the cleavage.

To further document the MMP-mediated cleavage sites on CD95L, we relied on the high resolution of a mass spectrometry (MS)-based approach. To this end, a series of five peptides (MS1–MS5) were designed to sequentially cover the entire stalk region and the beginning of the THD between positions 103 and 157 (Fig. 5A). In the N-terminal position of the peptides, a hexa-histidine tag was added and a spacer was intercalated between the tag and the sequence of interest (Table S2a). The specific design of these peptides was intended to obtain cleaved fragments of a size large enough (between 15 and 25 amino acids) to be detected by nanoLC–MS/MS. After MMP-mediated proteolysis of the five peptides, the cleaned-up fragments obtained were injected on either a Quadrupole Time-of-Flight (QTOF) or a nanoLC-coupled

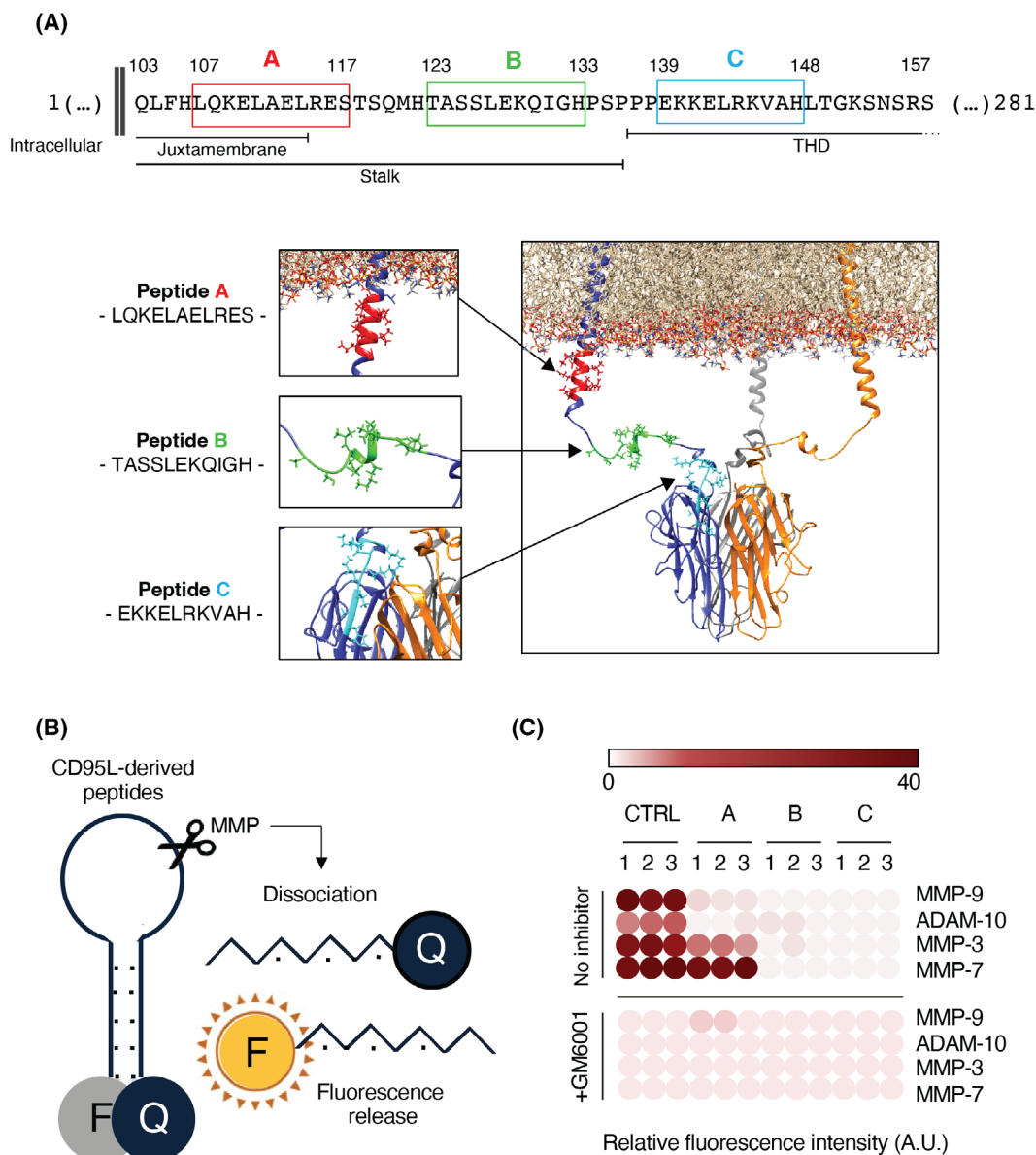


**Fig. 3.** CD95L fluorescent peptide cleavage assay. (A) Sequence and localization of peptides spanning the CD95L region targeted by metalloproteases previously described in the literature. Three peptides were designed and their sequence was highlighted on a trimeric model of CD95L to simulate the conformation and localization of the corresponding amino acids on the TM protein model. The model was rendered using the *SCHRÖDINGER* software. (B) Schematic representation of the fluorescent peptide proteolysis assay. A quencher (Q; Dnp) and a fluorophore (F; Mca) were coupled on opposite ends of the CD95L peptidic sequences. Proteolysis by metalloproteases lifts the quenching of the fluorophore by allowing the release of the cleaved peptide coupled with the quencher. Fluorescence is detected on a spectrofluorometer. (C) Proteolytic activity of the endopeptidases described in the literature (MMP-3, MMP-7, MMP-9 and ADAM-10) on peptides A, B and C. A pan-metalloprotease cleavable peptide (OMNIMMP) was used as a positive control. Relative fluorescence intensities were normalized to the baseline fluorescence of the corresponding undigested peptide. A parallel analysis was performed with the addition of the broad-spectrum metalloprotease inhibitor (GM6001) showing a complete inhibition of cleavage by metalloprotease. Experiments were conducted in triplicates.

TimsTOF Pro mass spectrometer, both coupled to a nanoLC system. Cleavage sites were detected by data-base driven peptide identification and chromatograms

were extracted from identified ions (Fig. 5B, Fig. S2a, b). All cleavage fragments detected by the QTOF (corresponding to sites  $_{106}\text{HL}_{107}$ ,  $_{113}\text{EL}_{114}$ ,  $_{142}\text{EL}_{143}$ ,

<sup>148</sup>HL<sub>149</sub>) were confirmed by the TimsTOF Pro (Fig. 5C, Fig. S2a, Table S2b). In addition, analyses on the TimsTOF Pro allowed us to identify seven additional fragments, corresponding to sites <sup>103</sup>QL<sub>104</sub>, <sup>104</sup>LF<sub>105</sub>, <sup>109</sup>KE<sub>110</sub>, <sup>110</sup>EL<sub>111</sub>, <sup>126</sup>SL<sub>127</sub>, <sup>138</sup>PE<sub>139</sub>, <sup>139</sup>EK<sub>140</sub> (Fig. 5C, Table S2b). Chromatographic profiles of the samples obtained from MMP-treated or untreated samples were compared, and the peaks exclusively detected in MMP-treated sample profiles were identified as resulting from MMP-mediated cleavage products. The five sites <sup>106</sup>HL<sub>107</sub>, <sup>113</sup>EL<sub>114</sub>, <sup>126</sup>SL<sub>127</sub>, <sup>142</sup>EL<sub>143</sub> and <sup>148</sup>HL<sub>149</sub> resulted in high-intensity peaks on the chromatograms (Fig. S2a), whereas the remaining six sites (<sup>103</sup>QL<sub>104</sub>, <sup>104</sup>LF<sub>105</sub>, <sup>109</sup>KE<sub>110</sub>, <sup>110</sup>EL<sub>111</sub>, <sup>138</sup>PE<sub>139</sub> and <sup>139</sup>EK<sub>140</sub>) were associated with low-intensity peaks. Overall, these fragments are the result of a proteolytic process by MMPs and describe the pair of amino acids corresponding to the potential cleavage site on the ectodomain sequence of CD95L. No fragmentation was detected for peptide MS2, meaning that no cleavage occurred in this amino acid region of CD95L ectodomain (Fig. S2b). The whole set of fragments found by MS thus allowed the mapping of CD95L cleavage region (Fig. 6). In conclusion, we identified 11 cleavage sites in our study, only 4 of which were reported in the literature (Figs 4A, 5C).

Five of the 11 identified sites were targeted by all 4 MMPs (MMP-2, MMP-3, MMP-7, MMP-12; Fig. 5C, Table S2b). One of these sites was detected using both proteomic approaches and was mapped between positions E<sub>113</sub> and L<sub>114</sub> of the protein. Therefore, we explored the possibility of blocking CD95L cleavage following mutation of the <sup>113</sup>EL<sub>114</sub> site. Thus, a mutated version of the molecular beacon peptide A was synthesized (<sup>113</sup>EL<sub>114</sub> to <sup>113</sup>AA<sub>114</sub> substitutions) (Fig. 7A). In contrast to the wild-type peptide, no fluorescence was detected upon incubation of the mutant peptide by any of the four MMPs tested (Fig. 7B). These results show that alteration of the peptide A [wild-type (WT)] sequence (at position <sup>113</sup>EL<sub>114</sub>) can prevent MMP-2, -3, -7 and -12-mediated cleavage of CD95L.

To further confirm the observations made *in vitro*, we either overexpressed the wild-type CD95L or the <sup>113</sup>EL<sub>114</sub> to <sup>113</sup>AA<sub>114</sub> variant in CD95 knockout (KO) HEK293T cells (Fig. 8A,B). Both forms were expressed at comparable levels and treatment with the protease inhibitor GM6001 prevented endogenous proteolysis of CD95L. Next, we co-expressed wild-type or variant CD95L with the soluble proteases identified above. We confirmed that in their native forms MMP-2, MMP-3, MMP-7, MMP-12 were able to cleave the

membrane-bound CD95L and that the <sup>113</sup>AA<sub>114</sub> mutation decreased the proteolytic efficiency of these proteases (Fig. 8D,E). In addition, we overexpressed a selection of membrane-type proteases (MMP-14, MMP-15 and ADAM-17). Similarly, we showed that in their membrane-bound form MMP-14, MMP-15 and ADAM-17 were able to cleave CD95L and that the alanine mutant decreased the CD95L cleavage efficiency.

## Discussion

CD95L/CD95 signalling has long been recognized as a key controller of tissue homeostasis. An increasing amount of literature reports that soluble form(s) of CD95L, accumulate in the bloodstream in various pathological conditions, which favours auto-immune, inflammatory diseases and cancers [12,17]. These sCD95L forms are, in most cases, poor apoptosis inducers but can drive nonapoptotic signalling outcomes, such as cell migration, or gene expression [8,56]. While this remains to be unequivocally proven in each of these individual pathologies, the accumulation of sCD95L has been suggested to contribute to disease severity [57]. Therefore, therapeutic targeting of sCD95L might be relevant in a broad range of pathologies. However, the exact form(s) of sCD95L which accumulates in the bloodstream of patients suffering from these conditions has not been defined. Furthermore, a systematic *in vitro* study of the MMPs responsible for the cleavage of CD95L and corresponding sites was never undertaken.

Herein, we used a combination of biochemical and MS-based approaches and demonstrate that in such conditions, both MMP-3 and MMP-7 systematically cleave CD95L as previously reported [15,17]. However, we could not detect CD95L cleavage by the membrane-tethered sheddase ADAM-10 previously reported to be involved in CD95L proteolysis. The *in vitro* approach used herein may not be the most appropriate to detect proteolysis by membrane-tethered proteases. This was confirmed by the observed ADAM-17, MMP-14 and MMP-15-mediated proteolysis of CD95L in a cellular system. We also provide solid evidence that two additional MMPs (i.e. MMP-2 and MMP-12) are also implicated in CD95L cleavage, an observation not reported before. The redundancy of MMP-mediated cleavage has been described for many substrates and may explain the absence of strong phenotypes in individual MMP knock-out in mice [58]. Nonetheless, the observation that CD95L is cleaved by many metalloproteases either soluble or membrane-anchored may be indicative of key biological functions



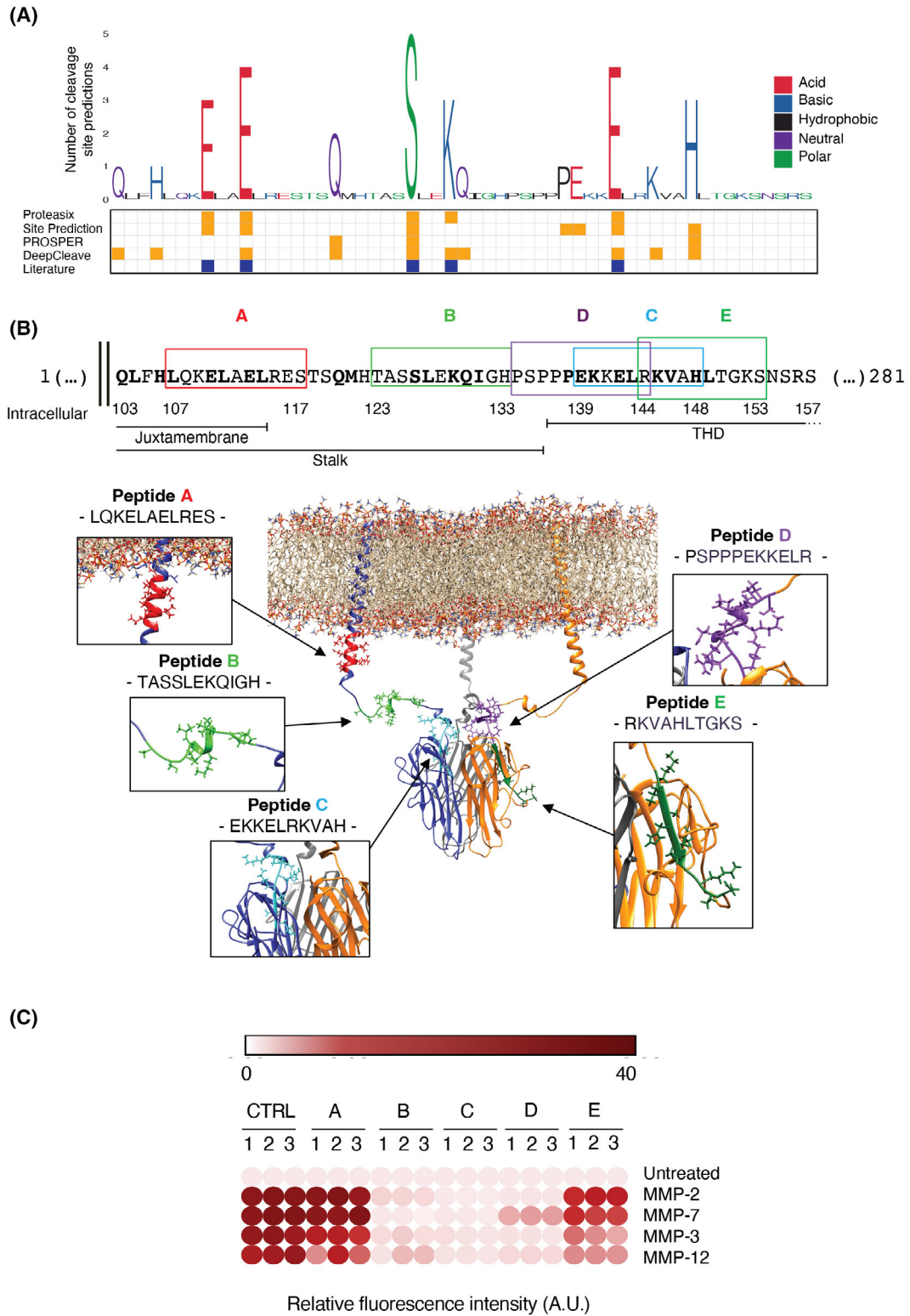


**Fig. 4.** Identification of new CD95L cleavage sites. (A) Weblogo representation of the frequency of the cleavage sites considered in the study. The size of the letter represents the number of times the cleavage site was predicted herein, or described in the literature (the latter shown with blue square). The cleavage sites targeted by MMP-2, MMP-3, MMP-7 and MMP-12, obtained from the proteolysis prediction tools (PROTEASIS, SITE PREDICTION, PROSPER, DEEPCLEAVE) are marked with yellow squares. For each *in silico* tool, only the predicted cleavage sites between amino acids 103–153 of the CD95L ectodomain were considered. (B) Design and localization of two additional peptides (Peptides D violet and E dark green) covering the region adjacent to the trimerization domain of CD95L. Peptides A, B and C are also indicated. The sequences of the five peptides are highlighted on a trimeric model of CD95L. The model was rendered using the SCHRÖDINGER software. (C) Proteolytic activity of the four endopeptidases cleaving IgCD95L and GST-CD95L (MMP-2, MMP-3, MMP-7, MMP-12) (Figs 1B, 2A) performed on Peptides A, B, C, D and E. Relative fluorescence intensities were normalized to the baseline fluorescence of the corresponding undigested peptide. A pan-metalloprotease cleavable peptide (OMNIMMP) was used as a positive control. Experiments were conducted three times.

associated with cleaved CD95L. Increased levels of sCD95L have been reported in the serum of Systemic Lupus Erythematosus (SLE) patients and patients with various cancers [13]. In addition, cellular overexpression and elevated serum levels of these four endopeptidases were observed in a wide variety of pathologies in which CD95/CD95L signalling has also been shown to contribute. For instance, MMP-2/MMP-3/MMP-7 serum levels are significantly increased in SLE and associated with disease activity, while elevated serum levels of MMP-12 have been observed in other systemic autoimmune diseases such as rheumatoid arthritis and systemic sclerosis [59–62]. MMP-2, -3, -7 and -12 have been reported to be overexpressed and associated with tumour propagation and poor cancer prognosis [59–71]. Thus, MMP deregulation in diseases might yield different forms of sCD95L, thereby resulting in abnormal CD95 signalling, which in turn could produce undesirable effects associated with the disease in question.

Moreover, we mapped two main proteolytic cleavage regions in CD95L located in the juxtamembrane region (aa 103–114) with six cleavage sites identified, and in the N-terminal region of the trimerization domain (aa 138–149) with four sites identified respectively (Fig. 6, Table S2b). Our results show that most of the sites are targeted by all four metalloproteases. The variety of cleavage sites identified might participate in the production of multiple isoforms of soluble CD95L. Homotrimers of each of these forms could differentially affect the cellular response. Furthermore, the heterogeneity of the monomers might impact the CD95L hetero-oligomer stability. Since some of the sites we identified are cleaved by a reduced number of endopeptidases, some isoforms may preferentially be released under specific pathological contexts where these metalloproteases are overexpressed. Since the oligomerization status of CD95L impacts its biological activity, the heterogeneity of the cleavage sites might thus also affect the biological activity of the different isoforms.

## Materials and methods

### Cell lines and plasmids

HEK 239 T cells were obtained from ATCC (LGC Standards, Molsheim, France) and cultured in DMEM (Gibco™; Life Technologies, NY, USA) supplemented with 8% v/v heat-inactivated (56 °C for 30 min) FBS (Sigma Life Science, St. Louis, USA) and 2 mM L-glutamine at 37 °C in a 5% CO<sub>2</sub> incubator. CD95 KO HEK293T cells were generated as described previously [72]. Since the KO was not complete cells were labelled with an anti-CD95<sub>PE</sub> antibody (clone DX2 BD Biosciences, Le Pont de Claix, France). CD95-negative cells were enriched using a BD FACSAria Fusion cell sorter (BD Biosciences). Recombinant CD95L constructs encoding the amino acids 103 to 281 from the soluble CD95L in tandem with either the GST (pcDNA3.1(+)-GST-CD95L<sub>103–281</sub>) or the Ig-like domain of the gp190 receptor for the Leukaemia Inhibitory Factor (LIF) (pEDr-IgCD95L<sub>105–281</sub>) [50] were used for the soluble recombinant proteins production. The pcDNA3.1(+) empty vector was purchased from Life Technologies (Carlsbad, CA, USA). Constructs encoding the full length CD95L (pcDNA3.1(+)-CD95L), the <sub>113AA</sub><sub>114</sub> mutant (pcDNA3.1(+)-CD95L mut <sub>113AA</sub><sub>114</sub>) and the FLAG-tagged (pcDNA3.1(+)-(protease)-FLAG) soluble MMP-2, MMP-3, MMP-7, MMP-12 and membrane-bound MMP-14, MMP-15, ADAM-17 were purchased from GenScript Biotech (Rijswijk, the Netherlands).

### Recombinant CD95L production in mammalian cells

Both GST and Ig recombinant CD95L were produced by transient overexpression in HEK 293 T cells. The transfection was carried out using the Calcium Phosphate method as described previously [73] using 3 µg of DNA. Cells were seeded at 1 million cells in 100 mm cell culture dish on Day 0, transfected on Day 1 and the culture medium was replaced with serum-free Opti-MEM supplemented with 2 mM L-glutamine on Day 2. Supernatants were collected 6 days after transfection (Day 7) and concentrated by centrifugation (4000 g/15 min/15 mL) using Amicon™ Ultra-15 Centrifugal

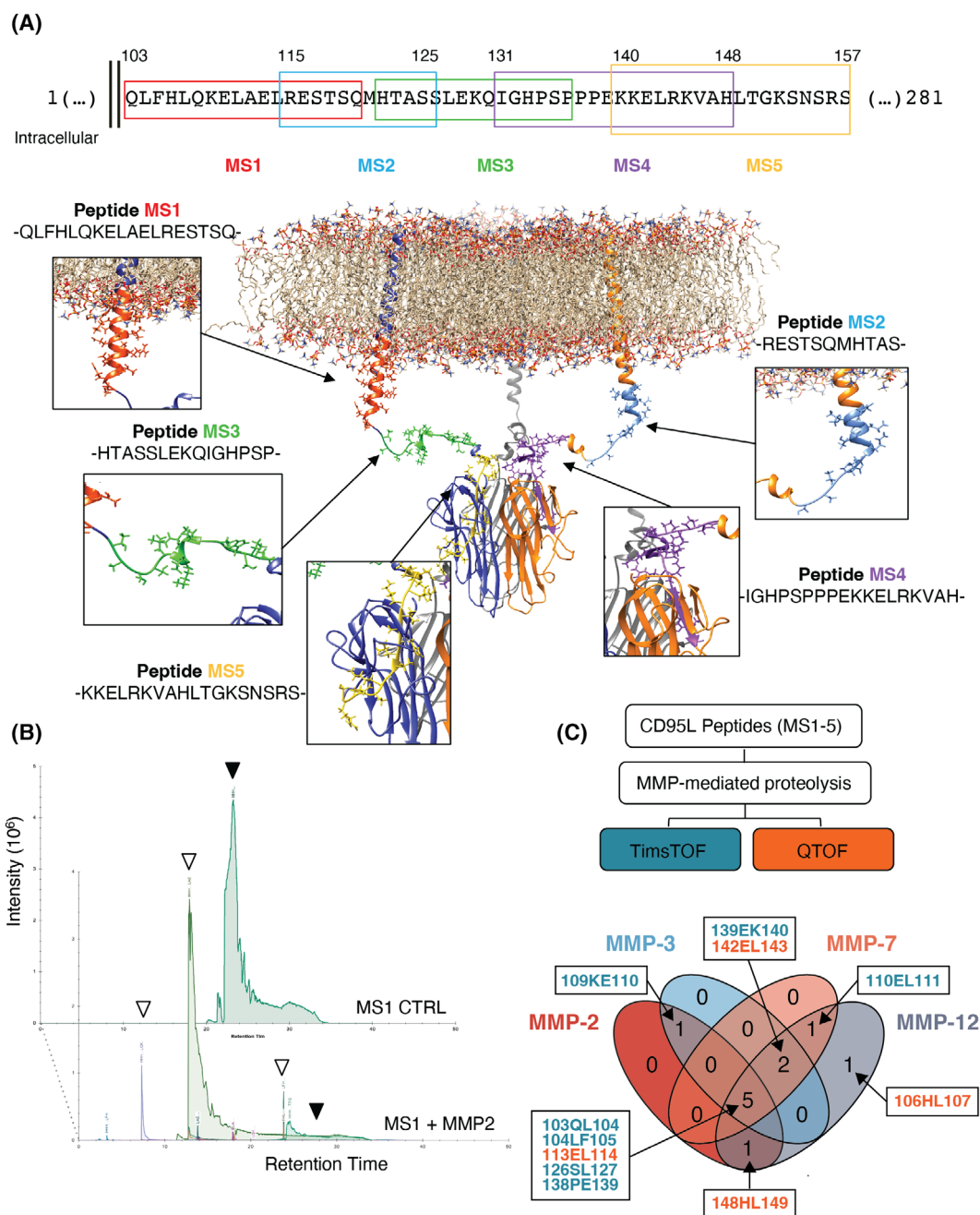


**Fig. 5.** Mass spectrometry-based characterization of the MMP-mediated cleavage of CD95L. (A) Sequence and localization of peptides intended for MS detection, spanning the region of CD95L where cleavage was detected by fluorometric assay. The five peptides (MS1-red, MS2-blue, MS3-light green, MS4-violet and MS5-yellow) are highlighted on a trimeric model of CD95L to simulate the conformation and localization of the corresponding amino acids on the TM protein. The model was rendered using the SCHRÖDINGER software. (B) Overlap of the LC chromatographic profiles extracted from uncleaved or MMP-2-digested peptide MS1 signal analysed by nanoLC-Tims TOF Pro. Peaks corresponding to undigested (black arrows) or MMP-2-cleaved fragments (light arrows) are indicated. (C) Venn Diagram representation of the cleavage sites detected using the two MS approaches (TimsTOF – blue, QTOF – orange) after digestion of peptides MS 1 to 5 with the four endopeptidases (MMP-2 – red, MMP-3 – blue, MMP-7 – orange and MMP-12 – grey). Most cleavage sites are identified in intersection areas as being targeted by more than one or all four metalloproteases. Only one cleavage site ( $_{106}$ HL $_{107}$ ) is targeted by a single metalloprotease (MMP-12). All cleavage sites identified by the QTOF spectrometer are equally identified by the TimsTOF spectrometer.

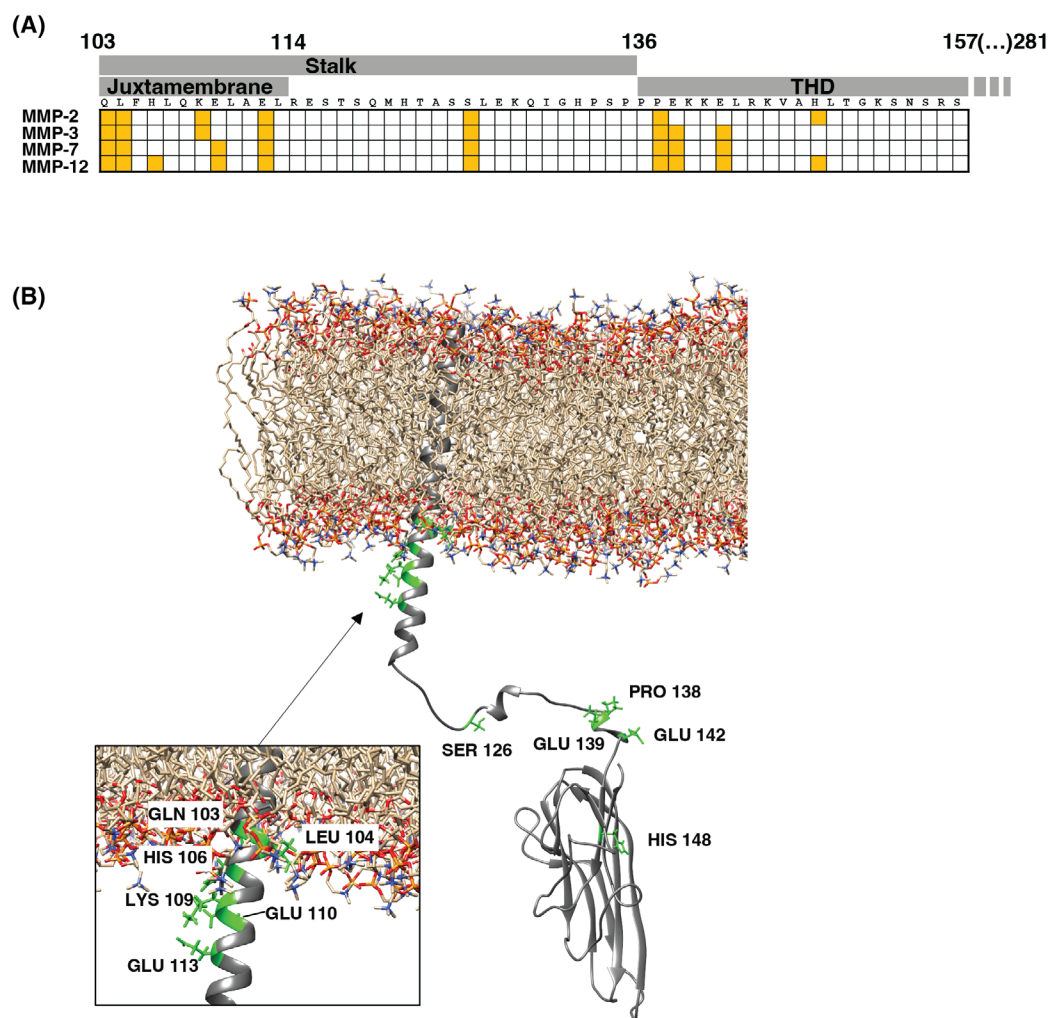


**Fig. 6.** Schematic representation of the CD95L ectodomain with the identified cleavage sites. (A) Localization of all cleavage sites detected by MS. The yellow square indicates the endopeptidase activity. The juxtamembrane and the THD domains are indicated. (B) Localization of all cleavage sites detected by MS mapped onto a monomeric model of CD95L. The first amino acid (P1 position) of each detected cleavage site is highlighted in the 3D model using the SCHRÖDINGER software.

Filter Units (Merck Millipore, Molsheim, France). Supernatant of HEK 293 T cells transfected with the pcDNA3.1(+) empty vector was used as a negative control. Recombinant GST-CD95L<sub>103–281</sub> and Ig-CD95L<sub>105–281</sub> were quantified by ELISA using the Human CD178 ELISA KIT from Diaclone (Besancon, France). The samples were incubated for 2 h at R.T. in the wells of the microtitre strip plate, coated with a highly specific antibody for CD95L. Once binding between CD95L and capture antibody was complete, any excess component was removed by several washes. The biotinylated secondary anti-CD95L antibody was then added and the system was incubated for 1 h. Excess of unbound secondary antibody to CD95L was removed by three washes. The Streptavidin-Horseradish Peroxidase (HRP) conjugate solution was then added to each well and incubated for 30 min at R.T. Additional washing removed the excess conjugate. The

chromogen substrate TMB was added to the wells and a short incubation of 10–15 min protected from light was performed. H<sub>2</sub>SO<sub>4</sub> was used as a stop reagent by turning the resulting final product yellow. The absorbance was measured by microtiter plate reader (TECAN Infinite F200 PRO) at the fixed 450 and 600 nm wavelengths. ODs generated for each standard were adopted to form a standard curve, allowing us to determine CD95L concentrations in each sample (GST-CD95L<sub>103–281</sub>: 1 µg·mL<sup>-1</sup>; Ig-CD95L<sub>105–281</sub>: 10 µg·mL<sup>-1</sup>).

#### Full length WT and mutant CD95L coexpression with proteases in mammalian cells

Briefly, ( $2 \times 10^5$ ) CD95KO HEK293T cells were cotransfected with 500 ng of WT or mutant full-length CD95L and

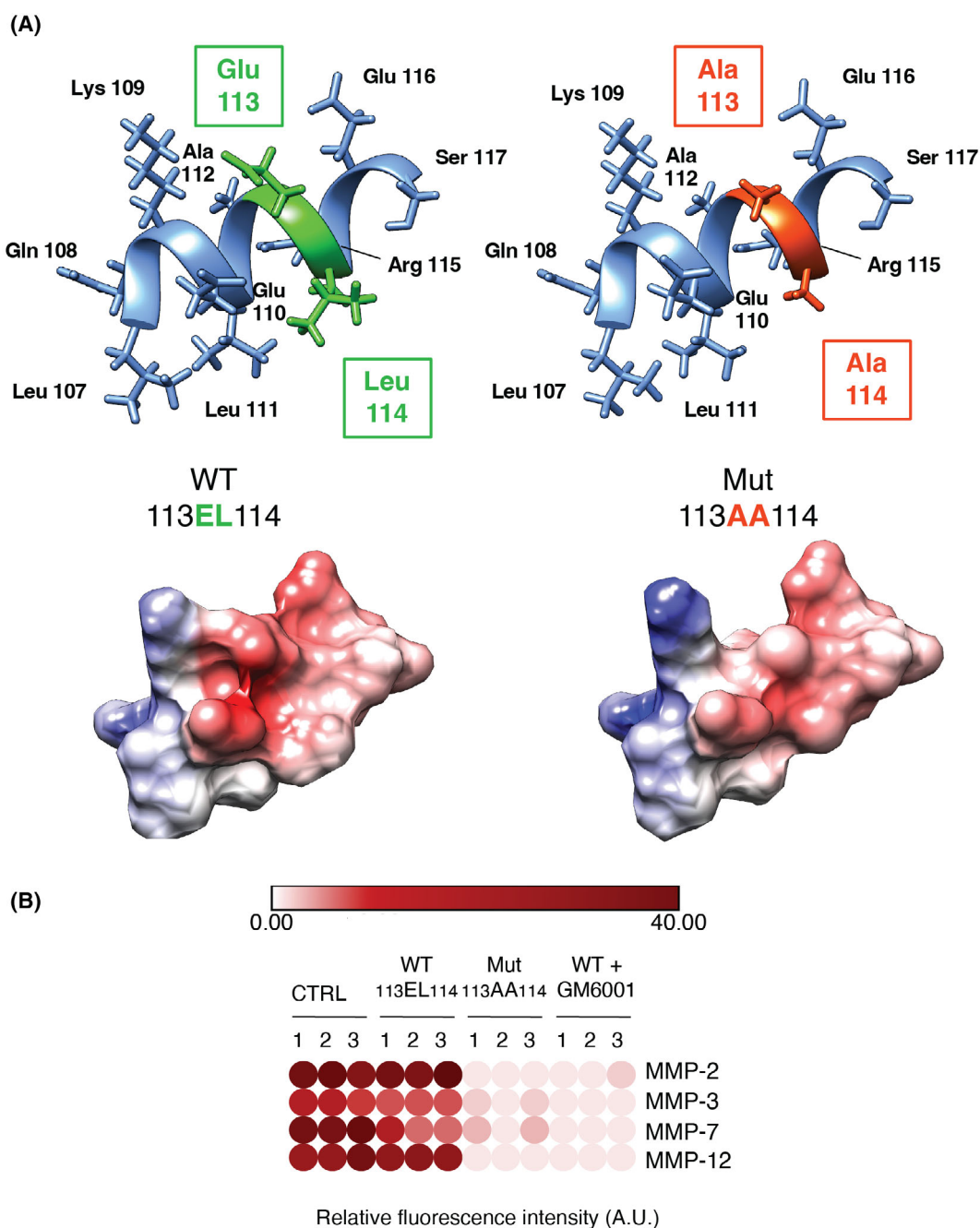


**Fig. 7.** Specific site mutagenesis impairs MMP-mediated cleavage of CD95L. (A) 3D modelling of the amino acid sequence 107–117 located in the ectodomain of CD95L and corresponding to the amino acid sequence used for the quenched fluorescent peptide A. In the upper left (WT  $_{113}EL_{114}$ /peptide A) the pair of amino acids targeted by the metalloproteases MMP-2, MMP-3, MMP-7 and MMP-12 is highlighted in green, while in the upper right (Mut  $_{113}AA_{114}$ ) the same pair of amino acids is replaced by two alanine residues highlighted in red. Below the alpha helices are the corresponding electrostatic surfaces of the two peptides, also illustrating the changes in topology. 3D models were created using the SCHRÖDINGER software. (B) Proteolytic activity of the endopeptidases cleaving IgCD95L and GST-CD95L (MMP-2, MMP-3, MMP-7 and MMP-12) (Figs 1B, 2A) on mutated peptide  $_{113}AA_{114}$  versus its progenitor WT $_{113}EL_{114}$  (Fig. 7A). Relative fluorescence intensities were normalized to the baseline fluorescence of the corresponding undigested peptide. Experiments were performed in triplicate. The analysis performed with the addition of the broad-spectrum metalloprotease inhibitor (GM6001) was used as negative control while a pan-metalloprotease cleavable peptide (OMNIMMP) was used as a positive control.

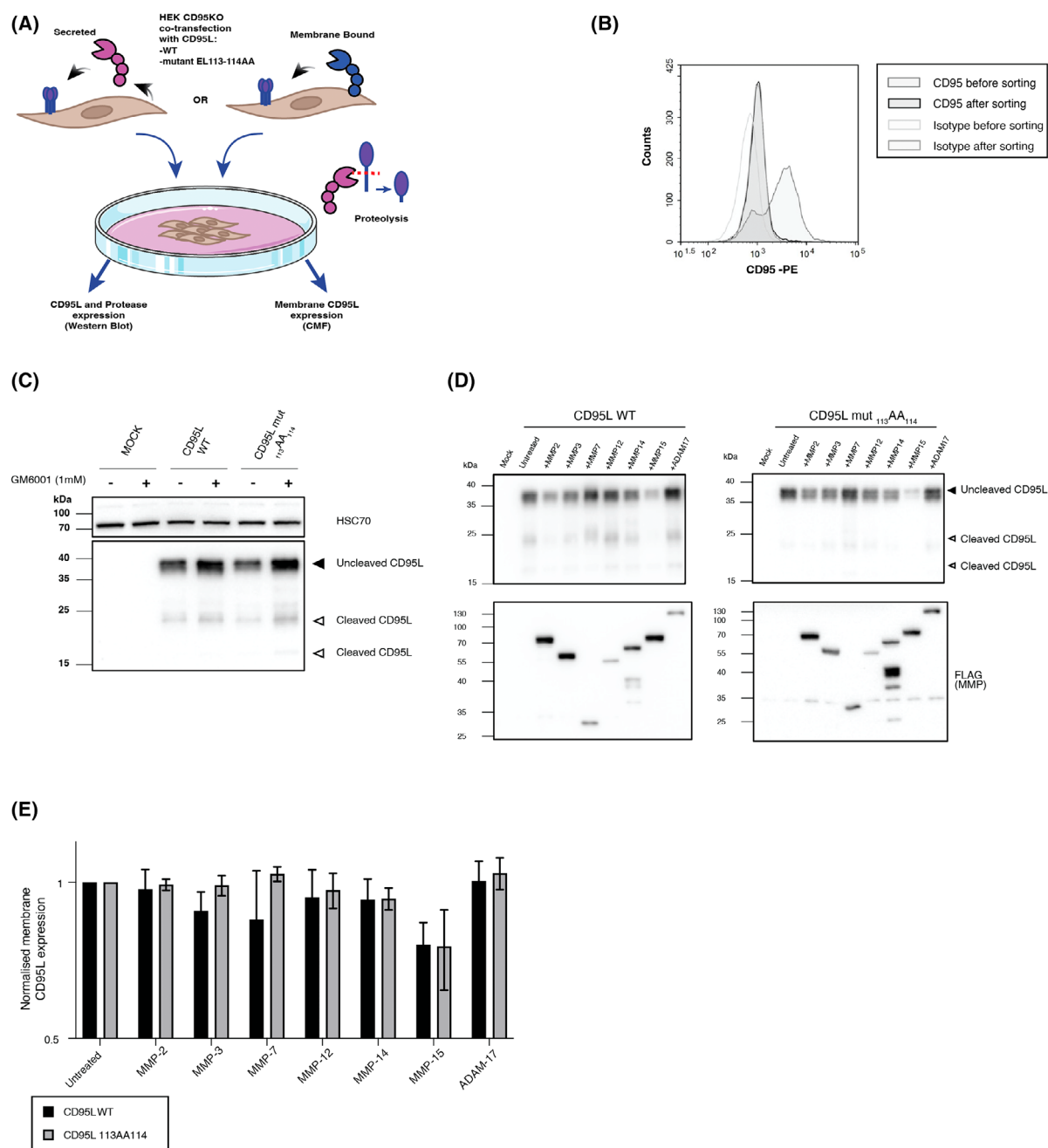


**Fig. 8.** *In cellulo* CD95L metalloprotease-mediated cleavage. (A) schematic representation of the experimental design. Full-length CD95L WT or 113AA<sub>114</sub> mutant was overexpressed in CD95 KO HEK293T cells with or without soluble (MMP-2, MMP-3, MMP-7, MMP-12) or membrane-bound proteases (MMP-14, MMP-15 and ADAM-17). (B) HEK293T CD95 KO cells membrane expression of CD95 before and after sorting was evaluated by flow cytometry after labelling with the mouse anti-human CD95-PE monoclonal antibody (clone DX2). Mouse IgG1-PE was used as an isotype control. (C) Lysates from CD95 KO HEK293T cells transfected with the WT or 113AA<sub>114</sub> mutant CD95L plasmid in the presence or absence of 1 mM GM6001 protease inhibitor were analysed by western blot using the indicated antibodies. HSC70 was used as a loading control. One experiment representative of three is shown. (D) Lysates from CD95 KO HEK293T cells cotransfected with the WT (left panel) or 113AA<sub>114</sub> mutant (right panel) CD95L plasmid and the indicated FLAG-tagged proteases encoding plasmids were analysed by western blot using the anti-CD95L or anti-FLAG antibodies. (E) CD95L surface expression from CD95 KO HEK293T cells cotransfected with the WT (black bars) or 113AA<sub>114</sub> mutant (grey bars) CD95L plasmid and the indicated FLAG-tagged proteases encoding plasmids was quantified by flow cytometry. Results are expressed as mean fluorescence intensity  $\pm$  SD normalized to the mock transfected control of four independent experiments.

500 ng of FLAG-tagged protease encoding plasmids in 6-well plates using the Calcium Phosphate method as described previously [72]. After 48 h cells were harvested and recombinant CD95L and metalloprotease expressions were assessed by immunoblotting on 20 µg of total protein. Membrane-bound CD95L expression was assessed by Flow cytometry.

### Metalloproteases and CD95L proteolysis assay

Metalloproteases were obtained from Merck Millipore (Molsheim, France) for MMP-2, MMP-3, MMP-7, MMP-8, MMP-9, MMP-13, ENZO Life Sciences (Villeurbanne, France) for MMP-1, MMP-12 and R&D Systems Europe – BIO TECHNE (Rennes, France) for MMP-14, MMP-15, MMP-17 ADAM-10 and ADAM-17. All enzymes were selected as active recombinant human form, consisting of the catalytic domain. The concentration of MMP used for the proteolysis of CD95L was customized as a function of the specific activity of each MMP for the substrate (Fig. S1a). To determine the optimal quantity of metalloproteases to be used for the proteolysis of recombinant soluble substrates, 150 µg of IgCD95L was digested with an increasing range (in units) of metalloproteases. Western blot analyses of proteolysis reactions were performed and image densitometry was used to estimate the quantity of cleaved IgCD95L (IMAGEJ software) (Fig. 1A, B, Fig. S1b). A nonlinear regression dose response model was fitted and EC50 ratios (MMP-2, MMP-3, MMP-12 and ADAM-10) or absolute IC50s (MMP-7, MMP-8, MMP-9, MMP-13, MMP-15 and MMP-17) were determined using GRAPHPAD PRISM 9.0.2 (Table S1a). These concentrations were maintained in the following immunoblot analyses. As for the substrates intended for fluorescence (10 µg) and MS (15 µg) analyses, the quantity of metalloproteases used for digestion was adapted as shown in Table S1b. The preparation of the samples was carried out at 4 °C to avoid the proteolytic preactivation of the MMPs on substrates. Then, the reaction was carried out at 37 °C for 1 h.

### Western blot analyses

Sample migration was performed using a 10% Tris-Glycine gel or 12% (cotransfection experiment) at 110 V for about 2 h, followed by a transfer on a nitrocellulose membrane using the Trans-Blot Turbo Transfer System (Bio-Rad, Hercules, CA, USA) or a liquid transfer (30 V, overnight) for the anti-FLAG immunoblot. The membrane was blocked for 30 min with TBST (50 mM Tris, 160 mM NaCl, 0.05% Tween 20, pH 7.8) containing 5% w/v skimmed milk powder or BSA (co-transfection experiment) and then incubated with an anti-CD95L primary antibody (clone D1N5E, rabbit mAb, Cell Signalling Technology, 1/2000 in BSA) an anti-FLAG antibody (DYKDDDDK Tag, rabbit mAb, Cell Signalling Technology, 1/2000 in BSA) or an

anti-HSC70 (B-6, mouse mAb, Santa Cruz Technology, 1/1000 in BSA) at 4 °C overnight. The membrane was washed twice with TBST and a HRP-conjugated Goat Anti-Rabbit secondary antibody (SouthernBiotech, Birmingham, USA) diluted to 1/4000 or Goat Anti-Rabbit secondary antibody (Dako) diluted to 1/7000 (cotransfection experiment) in TBST-BSA was added for 1 h. The signal was detected using the Intense Chemiluminescence Substrate Kit (ECL RevelBIOT Intense, Ozyme) or the ECL (SignalFire ECL Reagent, Cell Signalling Technology) (cotransfection experiment) on a G:Box Chemi XX6 imager from Syngene (Cambridge, UK).

### *In silico* cleavage predictions

Four different *in silico* tools (SitePrediction [52] <https://www.dnbr.ugent.be/prx/bioit2-public/SitePrediction/>, PROSPER [53] <https://prosper.erc.monash.edu.au/>, Proteasix [54] <http://proteasix.cs.man.ac.uk/tool.html>, DeepCleave [55] <https://deepcleave.erc.monash.edu.au/>) were used to predict cleavage sites on the extracellular CD95L amino acid sequence (i.e. aa 103–281). The FASTA sequence (UniProt-P48023|103–281) of the extracellular domain was used as an input for each of the four proteolytic prediction sites. Only human metalloproteases (hMMP-2, hMMP-3, hMMP-7, hMMP-12) were selected for cleavage prediction. The predicted cleavage sites included in the ectodomain region between residues 103 and 153 were selected. For SitePrediction, the only predicted sites with a confidence  $\geq 95\%$ , recognized around a sequence comprising six amino acids (P4 to P2') were selected. P1 and P1' positions correspond to the pair of amino acids between which the cleavage occurs. For DeepCleave, on the other hand, the threshold was set at 90% confidence, since this *in silico* tool performs more sensitive predictions including 8 amino acids around the cleavage site (P4 to P4'). The PROSPER instrument offers a general overview of the predicted cleavages for the metalloprotease family. Finally, Proteasix summarizes the cleavage sites described to date in the MEROPS peptidase database [74]. All this information has been added and the selection of 13 sites chosen for this study has been made (103QL<sub>104</sub>, 106HL<sub>107</sub>, 110EL<sub>111</sub>, 113EL<sub>114</sub>, 120QM<sub>121</sub>, 126SL<sub>127</sub>, 129KQ<sub>130</sub>, 130QI<sub>131</sub>, 138PE<sub>139</sub>, 139EK<sub>140</sub>, 142EL<sub>143</sub>, 145KV<sub>146</sub>, 148HL<sub>149</sub>).

### Sequence alignment

Sequences alignment of CD95L (UniProt-P48023) and TNF (UniProt-P01375) ectodomains was performed using the CLUSTAL OMEGA 1.2.4 software. The similarity scores were calculated according to the Gonnet PAM 250 matrix. The “\*” indicates fully conserved residues, the “:” indicates conservation between groups of strongly similar properties (scoring > 0.5). The “.” indicates conservation between groups of weakly similar properties (scoring  $\leq 0.5$ ).

## Peptide synthesis

Peptides were synthesized by two different providers SynPeptide (Shanghai, China) and Genscript (Leiden, the Netherlands) with a purity of greater than 95%. The quenched fluorescent peptides (FRET) series consists of six peptides, LQKELAELRES (Pept.A-WT<sub>113</sub>EL<sub>114</sub>/SynPeptide), LQKELAAARES (Pept.A-Mut<sub>113</sub>AA<sub>114</sub>/SynPeptide), TASSLEKQIGH (Pept.B/SynPeptide), EKKELRKVAH (Pept.C/SynPeptide), PSPPEKKELR (Pept.D/Genscript), RKVAHLTGKS (Pept.E/Genscript). These peptides were coupled with a C-Terminal quencher/acceptor Dnp (2,4-dinitrophenyl) and a N-terminal fluorophore/donor Mca (7-Methoxycoumarin-4-yl) acetyl (Table S1c). For MS analyses, a series of five peptides including an N-terminal histidine tag and a Linker/spacer interposed between the 6xHis Tag and the amino acid sequence, specifically chosen for each peptide sequence, were designed (MS1, MS2, MS3, MS4, MS5) (Table S2a) in order to obtain a post-cleavage fragment large enough to be detected by the mass spectrometer (between 15 and 25 residues). All of these peptides were synthesized by Genscript.

## Molecular beacon assay

After MMP-mediated proteolysis, the processed samples were exposed to radiation with controlled Excitation (Ex) and Emission (Em) wavelengths. The proteolytic process was carried out directly in black 96-well flat-bottom microplates (Greiner-Bio CELLSTAR). The functionality of the monochromators and the sensitivity of the filters of the Tecan Spark plate reader were chosen according to the characteristics of the control peptide (Ex: 328 nm; Em: 393 nm; optimal gain: 78). This control peptide can be cleaved by all MMPs (ENZO Life Sciences – OMNIMMP® fluorogenic substrate, BML-P126-0001). The cleavage of OMNIMMP by the different MMPs studied (MMP-2, MMP-3, MMP-7, MMP-12) takes place between the Glycine and Leucine on its consensus sequence Mca-P-L-G-L-Dpa-A-R-NH<sub>2</sub>.AcOH (Mca: 7-methoxycoumarin-4-yl) acetyl; Dpa: N-3-(2,4-dinitrophenyl)-L- $\alpha$ , $\beta$  diaminopropionyl. For the fluorescence assay 10  $\mu$ g (2  $\mu$ L) of the sample peptides, as well as the control peptide, were subjected to the proteolytic reaction. Three fluorescence intensity readings were made in each experiment and the average is reported. For each sample, the fluorescence intensity was measured both in basal conditions and in MMP-dependent cleavage conditions. Experiments were carried out in triplicates. A ratio of relative fluorescence intensities was calculated between the fluorescence intensity after the cleavage and the basal fluorescence intensity.

## Mass spectrometry analyses

Two MS systems were used to analyse the fragments obtained from the MMP-dependent cleavage of CD95L.

Both QTOF MS and Trapped Ion Mobility Spectrometry (TIMS) Time-Of-Flight (TOF) technologies were adopted for analysis of samples under basal condition and cleavage-dependent conditions. The peptide samples MS1, MS2, MS3, MS4, MS5 (15  $\mu$ g corresponding to 15  $\mu$ L) were processed with MMP-2, MMP-3, MMP-7 and MMP-12 for 1 h at 37 °C. In order to eliminate the large molecular weight contaminants, present in the postproteolysis final solution each sample was filtered through a 10-kDa membrane (Merck Amicon Ultra-0.5, Membrane Ultracel-10, PMNL 10 kDa) at 14 000 *g* for 35 min at 4 °C. Samples intended for analysis by TimsTOF underwent purification using a C18 reversed-phase chromatography Micro Spin Column (Harvard Apparatus, Cambridge, MA, USA) according to manufacturer's instructions. This phase was crucial to eliminate any saline contaminants, detergents and metalloprotease fragments derived from the proteolytic process. A Speed-Vac was then used to evaporate all the solvent containing acetonitrile (ACN) and obtain the dry product (45 °C/3 h). The dry final product was then resuspended in a liquid chromatography (LC) LOAD solution to the final concentration 1 mg·mL<sup>-1</sup>. Peptide mixtures were separated on a 75  $\mu$ m  $\times$  250 mm IonOpticks Aurora 2 C18 column (Ion Opticks Pty Ltd., Bundoora, Australia). A gradient of basic reversed-phase buffers (Buffer A: 0.1% FA, 98% H<sub>2</sub>O MilliQ, 2% ACN; Buffer B: 0.1% FA, 100% ACN) was run on a NanoElute HPLC System (Bruker Daltonik GmbH, Bremen, Germany) at a flow rate of 300 nL·min<sup>-1</sup> at 50 °C. The LC run lasted for 40 min (2–11% of buffer B during 19 min; up to 16% at 26 min; up to 25% at 30 min; up to 85% at 33 min and finally 85% for 7 min to wash the column). The column was coupled online with a TIMS TOF Pro (Bruker Daltonik GmbH, Bremen, Germany) with a Captive Spray ion source (Bruker Daltonik). The temperature of the ion transfer capillary was set at 180 °C. Ions were accumulated for 114 ms, and mobility separation was achieved by ramping the entrance potential from –160 V to –20 V within 114 ms. The acquisition of the MS and MS/MS mass spectra was done with average resolutions of 60 000 and 50 000 full widths at half maximum (mass range 100–1700 *m/z*) respectively. To enable the parallel accumulation-serial fragmentation (PASEF) method, precursor *m/z* and mobility information was first derived from full scan TIMS-MS experiments (with a mass range of *m/z* 100–1700). The quadrupole isolation width was set to 2 and 3 Th and, for fragmentation, the collision energies varied between 31 and 52 eV depending on the precursor mass and charge. TIMS, MS operation and PASEF were controlled and synchronized using the control instrument software OTOFCONTROL 5.1 (Bruker Daltonik). LC-MS/MS data were acquired using the PASEF method with a total cycle time of 1.31 s, including 1 TIMS MS scan and 10 PASEF MS/MA scans. The 10 PASEF scans (100 ms each) contain, on average, 12 MS/MS scans per PASEF scan. Ion mobility-resolved mass



spectra, nested ion mobility versus *m/z* distributions, as well as summed fragment ion intensities were extracted from the raw data file with DataAnalysis 5.1 (Bruker Daltonik GmbH, Bremen, Germany). Generated spectra were analysed with the Mascot database search engine (v2.5.1; <http://www.matrixscience.com>) for peptide identification, using its automatic decoy database search to estimate a false discovery rate (FDR) and calculate the threshold at which the *e*-values of the identified peptides were valid. According to the samples, the spectra were queried against a database containing the 5 peptides sequences (MS1, MS2, MS3, MS4, MS5). Mass tolerance for MS and MS/MS was set at 15 ppm and 0.05 Da respectively. No enzyme was selected. Identified peptides are validated with a score  $\geq 30$  at peptide spectrum match level, using PROLINE STUDIO v2.0.1 software [75] and chromatograms were extracted in Skyline-daily version 21.1.1.223 (University of Washington). Samples intended for analysis by QTOF underwent first a lyophilization step for 48 h. Processed samples were quickly frozen using liquid nitrogen and placed in the Alpha 2–4 LSC basic freeze dryer (Martin Christ Gefriertrocknungsanlagen GmbH, Germany) with the condenser previously set at  $-85^{\circ}\text{C}$ . The drying program was then inserted for 48 h with the application of vacuum (1 mbar). Samples were then analysed using an Acquity LC chromatographic system coupled in line with Xevo G2-XS QTOF mass spectrometer via an electrospray source (Waters, Milford, Massachusetts). Samples were dissolved in 50  $\mu\text{L}$  0.1% trifluoroacetic acid and 1  $\mu\text{L}$  was injected on a C18 Hypersil Gold column (150  $\times$  1 mm, ThermoScientific, San Jose, California) at 50  $\mu\text{L}\cdot\text{min}^{-1}$ . After 1 min at 2% ACN, 0.1% FA, a linear gradient from 2 to 20% ACN in 0.1% FA was applied in 19 min. The regeneration step and equilibration were performed in the next 10 min. The oven temperature was kept constant at 37.5  $^{\circ}\text{C}$ . The mass spectrometer was operated in positive ionization mode and data-dependent acquisition with a survey scan from *m/z* 300–2000. The three most intense multicharged ions from the survey scans were selected and fragmented with CID (Collision-Induced Dissociation). Raw data were first transformed in *mgf* files using PLGS 3.0.0 (Waters) and peptides were identified by database searching using SequestHT (Thermo Fisher Scientific) with PROTEOME DISCOVERER 2.4 software (Thermo Fisher Scientific). Precursor and fragment mass tolerances were set at 15 ppm and 0.05 Da, respectively, and no enzyme specificity was selected. Oxidation (+15.995, M) was set as variable modification. Peptides were filtered with a 1% FDR.

### CD95L modelling

The extracellular human CD95L structure was obtained by homology modelling using YASARA version 19.9.17 [76] using default settings, in order to resolve the noncrystallized region and thus generate a complete protein model.

The CD95L trimer (PDB: 4MSV) and the predicted structure from AlphaFold V2.0 (P48023) were used as templates. The obtained structure was prepared using Protein preparation wizard implemented in SCHRODINGER (Schrodinger Release 2021–3: Maestro, Schrodinger, LLC, New York, NY, 2021) and the membrane model (POPC, phosphatidylcholine) was set up between the amino acid 81 and 103.

### Membrane-bound CD95L flow cytometry detection

CD95L surface expression was determined by cell staining with anti-CD95L or isotype control antibodies. Briefly, 48 h post-transfection, ( $2 \cdot 10^5$ ) CD95 KO HEK293T cells were washed twice in PBS, blocked in ice-cold PBS with 2% SVF. Cells were then incubated for 30 min at 4  $^{\circ}\text{C}$  with an anti-CD95L-PE (NOK-1, mouse mAb), or the corresponding mouse IgG1-PE isotype antibody (BD Biosciences, Le pont de claux, France) in PBS-SVF buffer. Cells were then washed twice and resuspended in 50  $\mu\text{L}$  of PBS-SVF-BSA buffer. CD95L expression was assessed using an ACEA Novocyte 3000 flow cytometer (Agilent Technologies, Santa Clara, CA, USA).

### Acknowledgements

This work was funded by grants from the European Union's Horizon 2020 research and innovation program under grant agreement No 777995 to MLG, INCa (PLBIO2019) to ECh. This work was also supported by grants from Biogenouest, Infrastructures en Biologie Santé et Agronomie (IBiSA) and Conseil Régional de Bretagne awarded to C.P. the Swedish Research Council (2019-3684) to LAE and Sven and Lilly Lawski Foundation to MT. The Swedish National Infrastructure for Computing is acknowledged for generous allocations of computing time at supercomputing centres C3SE and NSC, in part funded by the Swedish Research Council through grant agreement no. 2018-05973.

### Conflict of interest

LAE is a founder of Cell Stress Discoveries Ltd, ECh is a founder of Thabor Therapeutics. The authors declare no conflict of interest.

### Author contributions

VR designed and performed experiments, contributed to the writing of the manuscript. MT, LAE contributed all the molecular modelling studies. LN, CP, BG, RL, EC performed MS analyses. EL contributed

to the writing of the manuscript, ECh supervised the work, raised funding, contributed to the writing of the manuscript. MLG supervised the work, raised funding, wrote the manuscript.

## Peer review

The peer review history for this article is available at <https://publons.com/publon/10.1111/febs.16737>.

## Data availability statement

The mass spectrometry proteomics data have been deposited to the ProteomeXchange Consortium via the PRIDE [1] partner repository with the dataset identifiers PXD039211, PXD039129 and [10.6019/PXD039129](https://doi.org/10.6019/PXD039129). The coordinates of the models (pdb format) are available for free download from Zenodo archive with the DOI: [10.5281/zenodo.7544325](https://doi.org/10.5281/zenodo.7544325).

## References

- Kischkel FC, Hellbardt S, Behrmann I, Germer M, Pawlita M, Krammer PH & Peter ME (1995) Cytotoxicity-dependent APO-1 (Fas/CD95)-associated proteins form a death-inducing signalling complex (DISC) with the receptor. *EMBO J* **14**, 5579–5588.
- Malinin NL, Boldin MP, Kovalenko AV & Wallach D (1997) MAP3K-related kinase involved in NF-kappaB induction by TNF, CD95 and IL-1. *Nature* **385**, 540–544.
- Alderson MR, Armitage RJ, Maraskovsky E, Tough TW, Roux E, Schooley K, Ramsdell F & Lynch DH (1993) Fas transduces activation signals in normal human T lymphocytes. *J Exp Med* **178**, 2231–2235.
- Chen L, Park SM, Tumanov AV, Hau A, Sawada K, Feig C, Turner JR, Fu YX, Romero IL, Lengyel E *et al.* (2010) CD95 promotes tumour growth. *Nature* **465**, 492–496.
- Peter ME, Hadji A, Murmann AE, Brockway S, Putzbach W, Pattanayak A & Ceppi P (2015) The role of CD95 and CD95 ligand in cancer. *Cell Death Differ* **22**, 549–559.
- Peters AMJ, Kohfink B, Martin H, Griesinger F, Wörmann B, Gahr M & Roesler J (1999) Defective apoptosis due to a point mutation in the death domain of CD95 associated with autoimmune lymphoproliferative syndrome, T-cell lymphoma, and Hodgkin's disease. *Exp Hematol* **27**, 868–874.
- Ta NL, Chakrabandhu K, Huault S & Hueber AO (2018) The tyrosine phosphorylated pro-survival form of Fas intensifies the EGF-induced signal in colorectal cancer cells through the nuclear EGFR/STAT3-mediated pathway. *Sci Rep* **8**, 12424.
- Tauzin S, Chaigne-Delalande B, Selva E, Khadra N, Daburon S, Contin-Bordes C, Blanco P, Le Seyec J, Ducret T, Counillon L *et al.* (2011) The naturally processed CD95L elicits a c-Yes/Calcium/PI3K-driven cell migration pathway. *PLoS Biol* **9**, e1001090.
- Malleter M, Tauzin S, Bessede A, Castellano R, Goubard A, Godey F, Levêque J, Jézéquel P, Campion L, Campone M *et al.* (2013) CD95L cell surface cleavage triggers a prometastatic signalling pathway in triple-negative breast cancer. *Cancer Res* **73**, 6711–6721.
- O'Reilly LA, Tai L, Lee L, Kruse EA, Grabow S, Fairlie WD, Haynes NM, Tarlinton DM, Zhang J-G, Belz GT *et al.* (2009) Membrane-bound Fas ligand only is essential for Fas-induced apoptosis. *Nature* **461**, 659–663.
- Poissonnier A, Sanséau D, Le Gallo M, Malleter M, Levoine N, Viel R, Morere L, Penna A, Blanco P, Dupuy A *et al.* (2016) CD95-mediated calcium signalling promotes T helper 17 trafficking to inflamed organs in lupus-prone mice. *Immunity* **45**, 209–223.
- Schneider P, Holler N, Bodmer J-L, Hahne M, Frei K, Fontana A & Tschopp J (1998) Conversion of membrane-bound Fas(CD95) ligand to its soluble form is associated with downregulation of its proapoptotic activity and loss of liver toxicity. *J Exp Med* **187**, 1205–1213.
- Risso V, Lafont É & Le Gallo M (2022) Therapeutic approaches targeting CD95L/CD95 signalling in cancer and autoimmune diseases. *Cell Death Dis* **13**, 248.
- Holler N, Tardivel A, Kovacs-Bankowski M, Hertig S, Gaide O, Martinon F, Tinel A, Deperthes D, Calderara S, Schulthess T *et al.* (2003) Two adjacent trimeric Fas ligands are required for Fas signalling and formation of a death-inducing signalling complex. *Mol Cell Biol* **23**, 1428–1440.
- Vargo-Gogola T, Crawford HC, Fingleton B & Matrisian LM (2002) Identification of novel matrix metalloproteinase-7 (matrilysin) cleavage sites in murine and human Fas ligand. *Arch Biochem Biophys* **408**, 155–161.
- Kirkin V, Cahuzac N, Guardiola-Serrano F, Huault S, Lückerrath K, Friedmann E, Novac N, Wels WS, Martoglio B, Hueber AO *et al.* (2007) The Fas ligand intracellular domain is released by ADAM10 and SPPL2a cleavage in T-cells. *Cell Death Differ* **14**, 1678–1687.
- Matsuno H, Yudoh K, Watanabe Y, Nakazawa F, Aono H & Kimura T (2001) Stromelysin-1 (MMP-3) in synovial fluid of patients with rheumatoid arthritis has potential to cleave membrane bound Fas ligand. *J Rheumatol* **28**, 22–28.
- Kiaei M, Kipiani K, Calingasan NY, Wille E, Chen J, Heissig B, Rafii S, Lorenzl S & Beal MF (2007) Matrix metalloproteinase-9 regulates TNF-alpha and FasL expression in neuronal, glial cells and its absence

- extends life in a transgenic mouse model of amyotrophic lateral sclerosis. *Exp Neurol* **205**, 74–81.
- 19 Schulte M, Reiss K, Lettau M, Marezky T, Ludwig A, Hartmann D, de Strooper B, Janssen O & Saftig P (2007) ADAM10 regulates FasL cell surface expression and modulates FasL-induced cytotoxicity and activation-induced cell death. *Cell Death Differ* **14**, 1040–1049.
  - 20 Biglari B, Büchler A, Swing T, Child C, Biehl E, Reitzel T, Bruckner T, Ferbert T, Korff S, Rief H *et al.* (2015) Serum sCD95L concentration in patients with spinal cord injury. *J Int Med Res* **43**, 250–256.
  - 21 Moghaddam A, Sperl A, Heller R, Gerner HJ & Biglari B (2016) sCD95L in serum after spinal cord injury. *Spinal Cord* **54**, 957–960.
  - 22 Lorente L, Martín MM, Ortiz-López R, González-Rivero AF, Pérez-Cejas A, Cabrera J, García C, Uribe L & Jiménez A (2020) Association between serum sFasL concentrations and sepsis mortality. *Infect Dis* **53**, 38–43.
  - 23 Kozłowski M, Kowalczyk O, Sulewska A, Dziegielewski P, Lapuc G, Laudanski W, Niklinska W, Chyczewski L, Niklinski J & Laudanski J (2007) Serum soluble Fas ligand (sFasL) in patients with primary squamous cell carcinoma of the oesophagus. *Folia Histochem Cytobiol* **45**, 199–204.
  - 24 Ding Y-W, Pan S-Y, Xie W, Shen H-Y & Wang H-H (2018) Elevated soluble Fas and FasL in cerebrospinal fluid and serum of patients with anti-N-methyl-D-aspartate receptor encephalitis. *Front Neurol* **9**, 904.
  - 25 Shiota G, Oyama K, Noguchi N, Takano Y, Kitaoka S & Kawasaki H (1998) Clinical significance of serum soluble Fas ligand in patients with acute self-limited and fulminant hepatitis. *Res Commun Mol Pathol Pharmacol* **101**, 3–12.
  - 26 Oliveira JB, Blesing JJ, Dianzani U, Fleisher TA, Jaffe ES, Lenardo MJ, Rieux-Laucat F, Siegel RM, Su HC, Teachey DT *et al.* (2010) Revised diagnostic criteria and classification for the autoimmune lymphoproliferative syndrome (ALPS): Report from the 2009 NIH International Workshop. *Blood* **116**, e35–e40.
  - 27 Caminha I, Fleisher TA, Hornung RL, Dale JK, Niemela JE, Price S, Davis J, Perkins K, Dowdell KC, Brown MR *et al.* (2010) Using biomarkers to predict the presence of FAS mutations in patients with features of the autoimmune lymphoproliferative syndrome. *J Allergy Clin Immunol* **125**, 946.
  - 28 De La Motte RT, Corné J, Cauchois A, Le Boulch M, Poupon C, Henno S, Rioux-Leclercq N, Le Pabic E, Laviolle B, Catros V *et al.* (2019) Serum CD95L level correlates with tumour immune infiltration and is a positive prognostic marker for advanced high-grade serous ovarian cancer. *Mol Cancer Res* **17**, 2537–2548.
  - 29 Molnár E, Radwan N, Kovács G, Andrikovics H, Henriquez F, Zerafov A, Hayman M, Linzner D, Thrasher AJ, Buckland M *et al.* (2020) Key diagnostic markers for autoimmune lymphoproliferative syndrome with molecular genetic diagnosis. *Blood* **136**, 1933–1945.
  - 30 D'Ortho MP, Will H, Atkinson S, Butler G, Messent A, Gavrilovic J, Smith B, Timpl R, Zardi L & Murphy G (1997) Membrane-type matrix metalloproteinases 1 and 2 exhibit broad-spectrum proteolytic capacities comparable to many matrix metalloproteinases. *Eur J Biochem* **250**, 751–757.
  - 31 English WR, Puente XS, Freije JMP, Knäuper V, Amour A, Merryweather A, López-Otín C & Murphy G (2000) Membrane type 4 matrix metalloproteinase (MMP17) has tumour necrosis factor-alpha convertase activity but does not activate pro-MMP2. *J Biol Chem* **275**, 14046–14055.
  - 32 Vandenbroucke RE, Dejonckheere E, Van Hauwermeiren F, Lodens S, De Rycke R, Van Wonterghem E, Staes A, Gevaert K, López-Otín C & Libert C (2013) Matrix metalloproteinase 13 modulates intestinal epithelial barrier integrity in inflammatory diseases by activating TNF. *EMBO Mol Med* **5**, 932.
  - 33 Lee E-J, Han JE, Woo M-S, Shin JA, Park E-M, Kang JL, Moon PG, Baek M-C, Son W-S, Ko YT *et al.* (2014) Matrix metalloproteinase-8 plays a pivotal role in neuroinflammation by modulating TNF- $\alpha$  activation. *J Immunol* **193**, 2384–2393.
  - 34 Churg A, Wang RD, Tai H, Wang X, Xie C, Dai J, Shapiro SD & Wright JL (2003) Macrophage metalloelastase mediates acute cigarette smoke-induced inflammation via tumour necrosis factor-alpha release. *Am J Respir Crit Care Med* **167**, 1083–1089.
  - 35 Gearing AJH, Beckett P, Christodoulou M, Churchill M, Clements J, Davidson AH, Drummond AH, Galloway WA, Gilbert R, Gordon JL *et al.* (1994) Processing of tumour necrosis factor-alpha precursor by metalloproteinases. *Nature* **370**, 555–557.
  - 36 Mezyk-Kopeć R, Bzowska M, Stalińska K, Chelmicki T, Podkalicki M, Jucha J, Kowalczyk K, Mak P & Bereta J (2009) Identification of ADAM10 as a major TNF sheddase in ADAM17-deficient fibroblasts. *Cytokine* **46**, 309–315.
  - 37 Tam EM, Morrison CJ, Wu YI, Stack MS & Overall CM (2004) Membrane protease proteomics: Isotope-coded affinity tag MS identification of undescribed MT1–matrix metalloproteinase substrates. *Proc Natl Acad Sci U S A* **101**, 6917.
  - 38 Secchiero P, Gonelli A, Corallini F, Ceconi C, Ferrari R & Zauli G (2010) Metalloproteinase 2 cleaves *in vitro* recombinant TRAIL: potential implications for the decreased serum levels of TRAIL after acute myocardial infarction. *Atherosclerosis* **211**, 333–336.
  - 39 Mohan MJ, Seaton T, Mitchell J, Howe A, Blackburn K, Burkhart W, Moyer M, Patel I, Waitt GM, Becherer JD *et al.* (2002) The tumor necrosis factor- $\alpha$  converting enzyme (TACE): a unique metalloproteinase

- with highly defined substrate selectivity. *Biochemistry* **41**, 9462–9469.
- 40 Murphy G & Nagase H (2008) Progress in matrix metalloproteinase research. *Mol Aspects Med* **29**, 290–308.
  - 41 Quintero-Fabián S, Arreola R, Becerril-Villanueva E, Torres-Romero JC, Arana-Argáez V, Lara-Riegos J, Ramírez-Camacho MA & Alvarez-Sánchez ME (2019) Role of matrix metalloproteinases in angiogenesis and cancer. *Front Oncol* **9**, 1370.
  - 42 Parks WC, Wilson CL & López-Boado YS (2004) Matrix metalloproteinases as modulators of inflammation and innate immunity. *Nat Rev Immunol* **4**, 617–629.
  - 43 Nabeshima K, Inoue T, Shimao Y & Sameshima T (2002) Matrix metalloproteinases in tumour invasion: role for cell migration. *Pathol Int* **52**, 255–264.
  - 44 Mannello F, Tonti GAM, Bagnara GP & Papa S (2006) Role and function of matrix metalloproteinases in the differentiation and biological characterization of mesenchymal stem cells. *Stem Cells* **24**, 475–481.
  - 45 Kessenbrock K, Wang CY & Werb Z (2015) Matrix metalloproteinases in stem cell regulation and cancer. *Matrix Biol* **44–46**, 184–190.
  - 46 Augustin S, Berard M, Kellaf S, Peyri N, Fauvel-Lafève F, Legrand C, He L & Crépin M (2009) Matrix metalloproteinases are involved in both type I (apoptosis) and type II (autophagy) cell death induced by sodium phenylacetate in MDA-MB-231 breast tumour cells. *Anticancer Res* **29**, 1335–1343.
  - 47 Lim CC, Liu PY, Tan HZ, Lee P, Chin YM, Mok IY, Chan CM & Choo JC (2017) Severe infections in patients with lupus nephritis treated with immunosuppressants: a retrospective cohort study. *Nephrology* **22**, 478–484.
  - 48 Black RA, Rauch CT, Kozlosky CJ, Peschon JJ, Slack JL, Wolfson MF, Castner BJ, Stocking KL, Reddy P, Srinivasan S *et al.* (1997) A metalloproteinase disintegrin that releases tumour-necrosis factor- $\alpha$  from cells. *Nature* **385**, 729–733.
  - 49 Moss ML, Jin S-LC, Milla ME, Burkhardt W, Carter HL, Chen W-J, Clay WC, Didsbury JR, Hassler D, Hoffman CR *et al.* (1997) Cloning of a disintegrin metalloproteinase that processes precursor tumour-necrosis factor- $\alpha$ . *Nature* **385**, 733–736.
  - 50 Daburon S, Devaud C, Costet P, Morello A, Garrigue-Antar L, Maillason M, Hargous N, Lapaillerie D, Bonneau M, Dechanet-Merville J *et al.* (2013) Functional characterization of a chimeric soluble Fas ligand polymer with *in vivo* anti-tumour activity. *PLoS One* **8**, 54000.
  - 51 Tanaka M, Itai T, Adachi M & Nagata S (1998) Downregulation of Fas ligand by shedding. *Nat Med* **4**, 31–36.
  - 52 Bordner AJ (2008) Predicting small ligand binding sites in proteins using backbone structure. *Bioinformatics* **24**, 2865–2871.
  - 53 Song J, Tan H, Perry AJ, Akutsu T, Webb GI, Whisstock JC & Pike RN (2012) PROSPER: an integrated feature-based tool for predicting protease substrate cleavage sites. *PLoS One* **7**, e50300.
  - 54 Klein J, Eales J, Züribig P, Vlahou A, Mischak H & Stevens R (2013) Proteasix: a tool for automated and large-scale prediction of proteases involved in naturally occurring peptide generation. *Proteomics* **13**, 1077–1082.
  - 55 Li F, Chen J, Leier A, Marquez-Lago T, Liu Q, Wang Y, Revote J, Smith AI, Akutsu T, Webb GI *et al.* (2020) DeepCleave: a deep learning predictor for caspase and matrix metalloprotease substrates and cleavage sites. *Bioinformatics* **36**, 1057–1065.
  - 56 Imamura R, Konaka K, Matsumoto N, Hasegawa M, Fukui M, Mukaida N, Kinoshita T & Suda T (2004) Fas ligand induces cell-autonomous NF-kappaB activation and interleukin-8 production by a mechanism distinct from that of tumour necrosis factor-alpha. *J Biol Chem* **279**, 46415–46423.
  - 57 Bossaller L, Rathinam VAK, Bonegio R, Chiang P-I, Busto P, Wespiser AR, Caffrey DR, Li Q-Z, Mohan C, Fitzgerald KA *et al.* (2013) Overexpression of membrane-bound Fas ligand (CD95L) exacerbates autoimmune disease and renal pathology in pristane-induced lupus. *J Immunol* **191**, 2104–2114.
  - 58 Löffek S, Schilling O & Franzke C-W (2011) Biological role of matrix metalloproteinases: a critical balance. *Eur Respir J* **38**, 191.
  - 59 Vira HJ, Pradhan VD, Umare VD, Chaudhary AK, Rajadhyksha AG, Nadkar MY, Ghosh K & Nadkarni AH (2020) Role of MMP-2 and its inhibitor TIMP-2 as biomarkers for susceptibility to systemic lupus erythematosus. *Biomark Med* **14**, 1109–1119.
  - 60 Vira H, Pradhan V, Umare V, Chaudhary A, Rajadhyksha A, Nadkar M, Ghosh K & Nadkarni A (2017) Role of MMP-7 in the pathogenesis of systemic lupus erythematosus (SLE). *Lupus* **26**, 937–943.
  - 61 Lee JM, Kronbichler A, Park SJ, Kim SH, Han KH, Kang HG, Ha IS, Cheong H, Kim KH, Kim G *et al.* (2019) Association between serum matrix metalloproteinase- (MMP-) 3 levels and systemic lupus erythematosus: a meta-analysis. *Dis Markers* **2019**, 9796735.
  - 62 Balog JA, Kemeny A, Puskas LG, Burcsar S, Balog A & Szebeni GJ (2021) Investigation of newly diagnosed drug-naive patients with systemic autoimmune diseases revealed the cleaved peptide tyrosine (PYY 3–36) as a specific plasma biomarker of rheumatoid arthritis. *Mediators Inflamm* **2021**, 5523582.
  - 63 He MK, Le Y, Zhang YF, Ouyang HY, Jian PE, Yu ZS, Wang LJ & Shi M (2018) Matrix metalloproteinase 12 expression is associated with tumour FOXP3 + regulatory T cell infiltration and poor prognosis in hepatocellular carcinoma. *Oncol Lett* **16**, 475–482.

- 64 Ella E, Harel Y, Abraham M, Wald H, Benny O, Karsch-Bluman A, Vincent D, Laurent D, Amir G, Izhar U *et al.* (2018) Matrix metalloproteinase 12 promotes tumour propagation in the lung. *J Thorac Cardiovasc Surg* **155**, 2164–2175.e1.
- 65 Jiang H & Li H (2021) Prognostic values of tumoral MMP2 and MMP9 overexpression in breast cancer: a systematic review and meta-analysis. *BMC Cancer* **21**, 149.
- 66 Azevedo Martins JM, Rabelo-Santos SH, Do Amaral Westin MC & Zeferino LC (2020) Tumoral and stromal expression of MMP-2, MMP-9, MMP-14, TIMP-1, TIMP-2, and VEGF-A in cervical cancer patient survival: a competing risk analysis. *BMC Cancer* **20**, 660.
- 67 Li H, Qiu Z, Li F & Wang C (2017) The relationship between MMP-2 and MMP-9 expression levels with breast cancer incidence and prognosis. *Oncol Lett* **14**, 5865–5870.
- 68 Mehner C, Miller E, Nassar A, Bamlet WR, Radisky ES & Radisky DC (2015) Tumour cell expression of MMP3 as a prognostic factor for poor survival in pancreatic, pulmonary, and mammary carcinoma. *Genes Cancer* **6**, 480–489.
- 69 Ibrahim FAER, Elfeky SE, Haroun M, Ahmed MAE, Elnaggar M, Ismail NAE & Abd El Moneim NA (2020) Association of matrix metalloproteinases 3 and 9 single nucleotide polymorphisms with breast cancer risk: a case–control study. *Mol Clin Oncol* **13**, 54–62.
- 70 Gobin E, Bagwell K, Wagner J, Mysona D, Sandirasegarane S, Smith N, Bai S, Sharma A, Schleifer R & She J-X (2019) A pan-cancer perspective of matrix metalloproteases (MMP) gene expression profile and their diagnostic/prognostic potential. *BMC Cancer* **19**, 1–10.
- 71 Liao HY, Da CM, Liao B & Zhang HH (2021) Roles of matrix metalloproteinase-7 (MMP-7) in cancer. *Clin Biochem* **92**, 9–18.
- 72 Guégan J-P, Pollet J, Ginestier C, Charafe-Jauffret E, Peter ME & Legembre P (2021) CD95/Fas suppresses NF- $\kappa$ B activation through recruitment of KPC2 in a CD95L/FasL-independent mechanism. *iScience* **24**, 103538.
- 73 Kwon M & Firestein BL (2013) DNA transfection: calcium phosphate method. *Methods Mol Biol* **1018**, 107–110.
- 74 Rawlings ND & Barrett AJ (1999) MEROPS: the peptidase database. *Nucleic Acids Res* **27**, 325–331.
- 75 Bouyssie D, Hesse AM, Mouton-Barbosa E, Rompais M, MacRon C, Carapito C, Gonzalez De Peredo A, Couté Y, Dupierris V, Burel A *et al.* (2020) Proline: an efficient and user-friendly software suite for large-scale proteomics. *Bioinformatics* **36**, 3148–3155.
- 76 Krieger E & Vriend G (2014) YASARA view – molecular graphics for all devices – from smartphones to workstations. *Bioinformatics* **30**, 2981–2982.

## Supporting information

Additional supporting information may be found online in the Supporting Information section at the end of the article.

**Table S1.** Specific activities and working concentrations of proteases.

**Table S2.** Mass spectrometry peptide sequences and cleavage sites.

**Fig. S1.** Specific activity of metalloproteases.

**Fig. S2.** Chromatographic profiles of cleaved peptides.